



## Review

# Metal or metal-containing nanoparticle@MOF nanocomposites as a promising type of photocatalyst



Yang Liu<sup>a,b,1</sup>, Zhifeng Liu<sup>a,b,1</sup>, Danlian Huang<sup>a,b,1</sup>, Min Cheng<sup>a,b,\*</sup>, Guangming Zeng<sup>a,b,\*</sup>, Cui Lai<sup>a,b</sup>, Chen Zhang<sup>a,b</sup>, Chengyun Zhou<sup>a,b</sup>, Wenjun Wang<sup>a,b</sup>, Danni Jiang<sup>a,b</sup>, Han Wang<sup>a,b</sup>, Binbin Shao<sup>a,b</sup>

<sup>a</sup> College of Environmental Science and Engineering, Hunan University, Changsha, Hunan 410082, China

<sup>b</sup> Key Laboratory of Environmental Biology and Pollution Control (Hunan University), Ministry of Education, Changsha, Hunan 410082, China

## ARTICLE INFO

## Article history:

Received 12 October 2018

Accepted 23 February 2019

## Keywords:

Photocatalysis

Metal-organic framework

Nanocomposites

Core-shell

Catalyst

## ABSTRACT

Photocatalysis is a promising technology that can convert solar energy into chemical energy. However, developing photocatalyst that could be put into the practical application remains a big challenge worldwide. In the recent years, an emerging type of core-shell/core-shell like composites, in which the metal or metal-containing nanoparticles (M/MC NPs) cores are encapsulated by the metal-organic frameworks (MOFs) shells, have attracted increasing attention in photocatalysis. These M/MC NP@MOF nanocomposites are believed to be one of the most effective and convenient ways to achieve property synergies of MOFs and M/MC NPs. Even though this field is currently in its infancy, the promising results obtained have validated the potential use of M/MC NP@MOF nanocomposites in practical applications. In this review, the fundamental mechanisms of photocatalysis were briefly introduced. The synthesis of M/MC NP@MOF nanocomposites and related photocatalytic applications (such as photocatalytic hydrogen generation and Cr(VI) reduction) are summarized and exemplified. Special emphasis is given to the synergistic effects between the MOFs shell and NPs core that result in an enhanced performance in heterogeneous photocatalysis. Finally, the unsolved problems of M/MC NP@MOF nanocatalysts are discussed and the future development prospects are proposed.

© 2019 Elsevier B.V. All rights reserved.

## Contents

1. Introduction	64
2. The fundamental mechanisms of photocatalysis	64
3. The synthetic strategies of M/MC NP@MOF nanocomposites	65
4. Metal NP@MOF for photocatalysis	66
5. Metal oxide NP@MOF for photocatalysis	69
5.1. TiO <sub>2</sub> NP@MOF	69
5.2. ZnO NP@MOF	69
5.3. Fe <sub>3</sub> O <sub>4</sub> NP@MOF	70
6. Other M/MC NP@MOF	72
7. Conclusions and prospects	74
Acknowledgements	75
References	75

\* Corresponding authors at: College of Environmental Science and Engineering, Hunan University, Changsha, Hunan 410082, China.

E-mail addresses: [chengmin@hnu.edu.cn](mailto:chengmin@hnu.edu.cn) (M. Cheng), [zgming@hnu.edu.cn](mailto:zgming@hnu.edu.cn) (G. Zeng).

<sup>1</sup> These authors contribute equally to this article.

## 1. Introduction

Heterogeneous catalysis is at the center of many industrial processes such as energy conversion, chemical manufacturing, oil refining, and pollution treatment [1–4]. Over the last two decades, the applications of heterogeneous photocatalysis have increased significantly. Heterogeneous photocatalysis is considered as a green technology, which has been successfully used to water splitting, environmental remediation and selective organic transformations operated under ambient conditions, i.e. atmospheric pressure and room temperature [5–9]. With the increasing concerns on the energy and environment problems, photocatalysis will play an even more important role. TiO<sub>2</sub> in the anatase form has been mostly investigated in the fields of energy generation and pollutant treatment due to its low production costs, high physical and chemical stability [10–12]. However, the applications of TiO<sub>2</sub> are greatly hindered by its wide band gap (3.2 eV) and high recombination of photogenerated electron-hole pairs, which results in the poor energy utilization efficiency for solar light and low quantum efficiency of photocatalytic reactions [13–15]. Therefore, the development of new photocatalyst that could be put into practical application remains a big challenge worldwide.

Metal-organic frameworks (MOFs), also known as coordination polymer networks (CPNs) or porous coordination polymers (PCPs), are a group of very promising porous crystalline inorganic-organic hybrid materials, have become one of the fastest growing fields in both materials science and chemistry in the last two decades [16–18]. MOFs not only combine the respective beneficial characteristics of metal ions and organic ligands but also often present unique properties that exceed the expectations for a simple mixture of the components [19–21]. Owing to their distinguished features such as modifiable organic linkers, tunable coordination space and adjustable internal surfaces, MOFs are of pronounced interest in diverse areas such as gas storage [22], sensing [23], separation [24], controlled guest release [25], and catalysis [26,27].

MOFs have shown great advantages for photocatalysis as a result of their flexible structure design and the unique physicochemical properties compared with traditional photocatalysts [28–34]. As the historic work made by Mahata and co-workers in 2006 [35], more and more efforts have been made to explore the MOFs as photocatalysts [16,36–40]. Many kinds of MOFs, such as MIL-53(Fe) [41], MIL-68(Fe) [42] and MIL-100(Fe) [43], were found have intensive absorption in the visible light region mainly because of the existence of metal-oxo clusters in their structures [44,45]. Further studies have shown that the photocatalytic performance of MOFs catalysts can be enhanced by combination with semiconductors, decoration of linker or metal center [26]. Among these, the fabrication of metal or metal-containing nanoparticles (M/MC NPs) into the MOFs photocatalysts has gained increasing attention [46,47]. These core-shell or core-shell-like (yolk-shell structures, within-the-pore structures and sandwich structures) nanocomposites are considered to be one of the most effective and convenient ways to achieve property synergies of MOFs and M/MC NPs for multifunctional applications [48]. M/MC NP@MOF nanocomposites often present excellent physical and chemical properties, such as multi-functionality, high stability and dispersibility. In the M/MC NPs@MOF nanocomposites, the advantages of both the M/MC NPs core (e.g., magnetic, electrical, catalytic properties, etc.) and MOFs shell (e.g., multi-coordination sites, ordered crystalline pores, structural adaptivity and flexibility, etc.) can be combined. The encapsulation of M/MC NPs cores within the MOFs shells can greatly enhance their stability against aggregation, and avoid undesirable dissolution or corrosion during the photocatalysis [49]. Compared to the other shell materials such as silica and metal oxides, MOFs have several advantages, which

include (1) they possess very high porosity and surface areas, which is desirable for hosting M/MC NPs; (2) the great diversity and abundance of MOFs structures and their tunable pore size and shapes can meet the particular requirements of different M/MC NPs; (3) the nanopores can provide confinement effects and shape selectivity; and (4) the proper organic linkers in MOFs structures can offer interaction with NPs [50–52]. As for the M/MC NPs core, its low lying Fermi energy level (especially for the noble metals) can serve as a reservoir of photoelectrons and prolong the lifetime of photo-generated charge carriers, thus enhancing the overall photocatalytic performance [53].

In the past few years, M/MC NP@MOF nanocomposites have attracted tremendous attention in heterogeneous photocatalysis because of their intriguing properties. The growing number of research articles on this topic indicates that M/MC NP@MOF nanocomposites will play an important role in heterogeneous photocatalysis. Several review papers [46,47,49,54–56] have already mentioned the application of M/MC NP@MOF nanocomposites in photocatalysis. As early as in 2013, Liu and Tang [49] have summarized the progress in the synthesis of multifunctional NP@MOF nanocomposites, and concluded that the multifunctional NP@MOF materials have enormous potential for medicine, energy, devices, and the environment applications. More recently, some researchers have summarized the preparation and characterization methods of metal NP@MOF nanocomposites as well as their applications in selective catalysis [47]. To the best of our knowledge, however, reviews outlining the M/MC NP@MOF nanocomposites for heterogeneous photocatalysis and the related mechanism have not been available. Therefore, a comprehensive review summarizing M/MC NP@MOF nanocomposites-based heterogeneous photocatalysis is highly expected.

Herein, we provide a tutorial review with aim to give an account of the fundamental aspects of M/MC NP@MOF-based heterogeneous photocatalysis. Section 2 describes the fundamental mechanisms of photocatalysis. Section 3 summarizes the synthetic strategies of M/MC NP@MOF nanocomposites. Sections 4–6 discuss the synthesis of different types of M/MC NP@MOF nanocomposites and their application in heterogeneous photocatalysis. Finally, the existing problems in this field and the future development prospects are proposed.

## 2. The fundamental mechanisms of photocatalysis

Photocatalysis is a complicated heterogeneous catalytic process, which is controlled by many factors. Extensive investigations have been conducted to study the critical factors for photocatalytic process and try to indicate the behind mechanisms [57–60]. Fig. 1 shows the schematic diagram of the well-recognized mechanism of photocatalytic process for semiconductors [61]. When a given photocatalyst is exposed to UV light or visible light with energy beyond its corresponding band gap energy ( $E_g$ ), the electrons ( $e^-$ ) on the valence band (VB) will be excited by the incident photon and spontaneously jump into the conduction band (CB) of the photocatalyst and leave the same number of holes ( $h^+$ ) in VB, resulting in the generation of photo-excited electron-hole pairs (Eq. (1)) [62]. The photo-generated  $e^-$  and  $h^+$  can then migrate to the surface of the photocatalyst, where they participate in redox reactions with adsorbed species, leading to the production of superoxide radical ( $O_2^-$ ) (Eq. (2)) and hydroxyl radical ( $\cdot OH$ ) (Eq. (3), (4)) [61,63]. In the case of photocatalytic degradation of organic pollutants, the pollutants (e.g., dyes, pesticides, antibiotics, etc.) can be degraded by  $\cdot OH$  generated on the VB (Eq. (5)), or directly oxidized by photo-excited  $h^+$  in the CB (Eq. (6)). As shown in Eq. (7), the photo-generated  $e^-$  can also be used for the reduction of highly toxic Cr(VI) into low-toxic form of Cr(III) [64]. When a photocat-

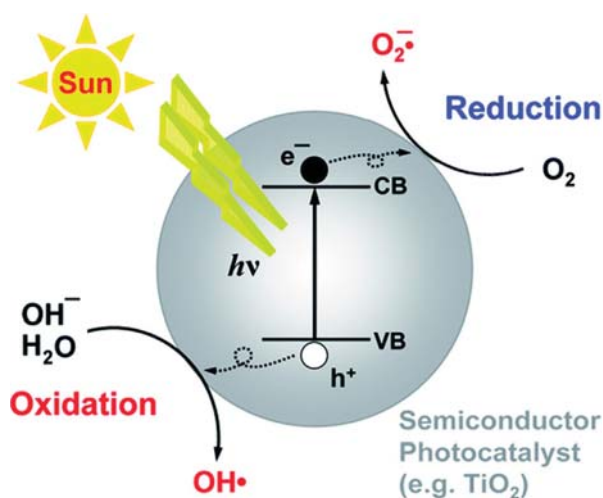


Fig. 1. Schematic diagram of the principle of photocatalysis. Reproduced with permission from Ref. [61]. Copyright 2014 The Royal Society of Chemistry.

lyst is used for water splitting, the VB value of the photocatalyst must be below the energy of the  $O_2/H_2O$  redox couple, and the CB value must be above the energy of the  $H^+/H_2$  redox couple [65–67]. Based on these,  $O_2$  and  $H_2$  could be produced via Eqs. (8) and (9), respectively. As for photocatalytic  $CO_2$  reduction, only the  $e^-$  with the sufficient reduction potential can be utilized for particular  $CO_2$  reduction reactions (Eqs. (10–14)) [68–71], while the holes in the VB are involved in water oxidation (Eqs. (8)) [72].

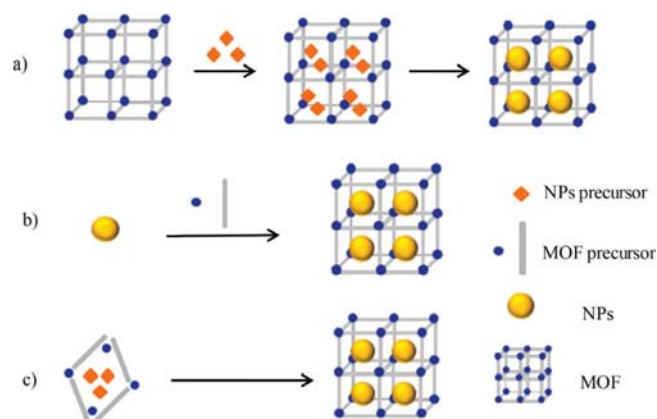
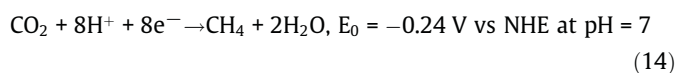
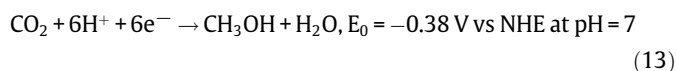
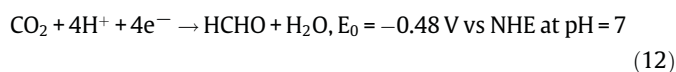
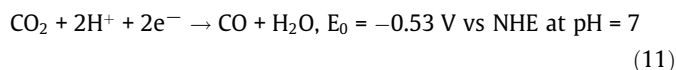
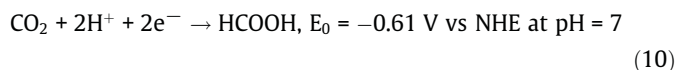
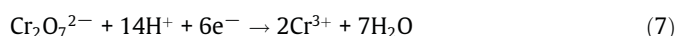
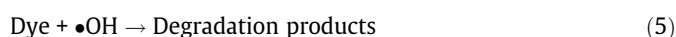
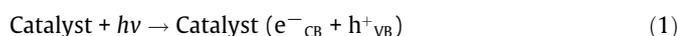
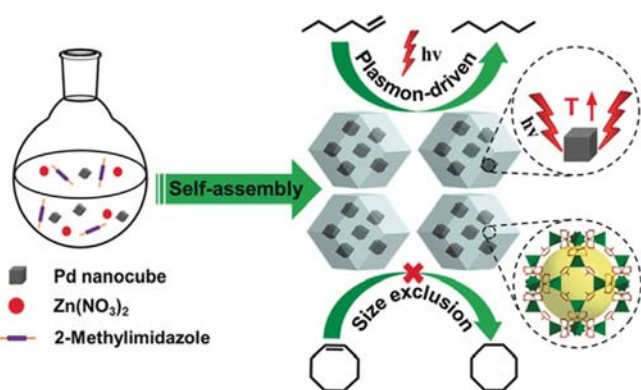


Fig. 2. Different synthetic approaches for the preparation of M/MC NPs@MOF nanocomposites: (a) the “ship-in-a-bottle” approach, (b) the “bottle-around-ship” approach, and (c) the “one-pot” approach. Reproduced with permission from Ref. [75]. Copyright 2017 MDPI.

### 3. The synthetic strategies of M/MC NP@MOF nanocomposites

Diverse synthetic methods to incorporate M/MC NPs into MOFs shells have been developed. Several excellent reviews have already summarized the preparation methods of M/MC NP@MOF nanocomposites [46,51,73,74]. For example, in a recent published work, Yang et al. [55] have systematically introduced the development of the synthetic approaches to the formation of M NPs/MOFs composites, and discussed the respective advantages as well as disadvantages of some specific approaches such as solution impregnation and chemical vapor deposition.

In general, the preparation of M/MC NP@MOF nanocomposites can be classified into four approaches, which were presented in Fig. 2 [75]. The first approach is the introduction of MOFs into a solution which contains the M/MC NPs precursors, followed by the formation of M/MC NPs inside the MOFs (Fig. 2a). This approach is also called the “ship-in-a-bottle” approach, which is expected to restrict the growth of M/MC NPs and prevent their agglomeration. Particle formation is subsequently triggered within the MOFs by the application of reducing agents, heat or radiation [46]. By using this method, the metallic and bimetallic NPs including Rh, Ni, Pt, Pd, CuCo, AuCo and AuNi have been successfully immobilized inside the pores of different types of MOFs without aggregation on the external surface of the framework [73,75–78]. However, some aspects of this methodology should be considered: 1) the precursors need to be compatible with the MOF structure; 2) the MOFs need to be stable under the conditions required to form the M/MC NPs; and 3) the M/MC NPs need to form within the framework rather than on the external surface of the MOFs. Moreover, it remains a significant challenge to precise control over the internal location, size, morphology and shape of the M/MC NPs within the MOFs structure. The second is the dispersion of pre-synthesized M/MC NPs into a reaction solution for subsequent MOFs synthesis (Fig. 2b), known as “bottle around ship” approach. It is obvious that the problems of the aggregation of M/MC NPs on the external surface of MOFs can be reduced by using the “bottle-around-ship” approach since the MOFs were assembled surround the M/MC NPs [50]. Besides, the size, morphology and shape of the M/MC NPs can be well-defined due to the fact that M/MC NPs were pre-formed. But, it should be noted that the growth of the MOFs in some cases may be difficult due to the high interfacial energy barrier between the two kinds of materials [75]. The third is the simultaneous formation of the two components to afford M/MC NP@MOF composites (Fig. 2c), known as the “one-pot” approach. This strategy involves mixing all the necessary



**Fig. 3.** Self-assembly of Pd nanocubes@ZIF-8 and plasmon-driven selective photocatalysis of the hydrogenation of olefins. Reproduced with permission from Ref. [105]. Copyright 2016 Wiley-VCH.

constituents (e.g., precursors of the MOFs and M/MC NPs) in solution, whereby the MOFs and M/MC NPs are generated simultaneously. When compared with the above two mentioned approaches, one-pot synthesis strategy is straightforward and simple, however, the synchronous control of the self-nucleation as well as the growth of MOFs and M/MC NPs is difficult and, as a result, the fabrication of the desired uniform M/MC NP@MOF nanocomposites by this strategy is not easy [73,74].

#### 4. Metal NP@MOF for photocatalysis

Metal NPs (M NPs), particularly noble metal NPs, have attracted intense attention in heterogeneous catalysis [79–82]. Unfortunately, several unavoidable factors associated with these NPs, for example, they are thermodynamically unstable and tend to aggregate during the continuous catalytic reactions, in order to reduce the surface energy [83–87]. Consequently, control of the dispersion of M NPs in the solution is a critical factor in achieving high and stable activity [88–90]. So far, the most common approaches are to load the noble metal NPs onto the outside or deliver them into the pores of certain support materials [79,91–97]. A new approach to enhance the catalytic performance of a M NPs catalyst is to fabricate the catalyst into a core-shell architecture, which consists of inner core (M NPs) encapsulated by porous shell materials [51,98,99]. Over the years, a variety of M NP@porous material nanocomposites have been developed with shell materials of polymers [100], metal oxides [101,102], carbon [103], silica [104], and MOFs [98]. Among these, the encapsulation of M NPs within MOFs shell for photocatalysis has received significant attention in recent years. Compared with other porous materials, MOFs can offer unique advantages for photocatalysis, for example, the great diversity of MOFs structures can provide confinement effects and size selectivity [51]. In 2016, Yang et al. [105] rationally designed and fabricated Pd nanocubes@ZIF-8 composites through a self-assembled method (Fig. 3), and applied them to selective catalytic hydrogenation of olefins under visible light irradiation. The results showed that the photocatalytic activity of Pd nanocubes@ZIF-8 is significantly enhanced as compared to Pd nanocubes. This enhancement is because ZIF-8 shell could promote the hydrogenation process by serving multiple roles: 1) ZIF-8 shell greatly boosts the catalytic efficiency by the H<sub>2</sub> enrichment effect; 2) the pore structure of ZIF-8 shell is beneficial to the transportation of substrates/products and guarantees the accessibility of the Pd active sites; and 3) ZIF-8 shell can act as a “molecular sieve” to differentiate olefins and therefore enables the size-selective hydrogenation (Fig. 3). The size-selective effect of MOFs has also been reported in several other works [99,106–111]. For instance, PtCo@UiO-66

core-shell catalysts were recently fabricated by Chang and Li [111] through a one-step method, and showed good size selectivity in olefins hydrogenation under room temperature. These works unambiguously presents the synergistic functions of the active noble metal NPs core and the size selectivity effect endowed by the MOFs shell.

In 2016, Li et al. [112] reported the encapsulation of Pd nanoclusters inside the cage of NH<sub>2</sub>-UiO-66(Zr) via a double-solvent approach combined with a photoreduction process (Fig. 4a). By successful coupling of the Pd catalysis with MOF-based photocatalysis, the as-prepared Pd@NH<sub>2</sub>-UiO-66(Zr) showed excellent performance for Suzuki coupling reaction under visible-light irradiations. It was demonstrated that Suzuki coupling reaction was promoted by the efficient electron transfer from the light-excited NH<sub>2</sub>-UiO-66(Zr) to the confined Pd nanoclusters (Fig. 4b). In a following work, they also fabricated Pd@MIL-100(Fe) through a similar approach [113]. The resultant Pd@MIL-100(Fe) showed much better performance in light-induced N-alkylation of amines with alcohols than Pd/MIL-100(Fe), in which Pd NPs were deposited on the external surface of MIL-100(Fe) [94]. More recently, PdAu@MIL-100(Fe) [114] and CuPd@NH<sub>2</sub>-UiO-66(Zr) [115] were synthesized by the same research group. In the first case, the as-formed bimetallic PdAu@MIL-100(Fe) present superior performance in light-induced N-alkylation reaction over the bare Pd@MIL-100(Fe), which was caused by the promoting effect of metallic Au in the photocatalytic dehydrogenation process [114]. In the second case, CuPd@NH<sub>2</sub>-UiO-66(Zr) showed superior performance for light-induced Suzuki coupling reaction as compared with Pd@NH<sub>2</sub>-UiO-66(Zr) [115]. As shown Fig. 5, the existence of metallic Cu can promote the electron transfer from excited NH<sub>2</sub>-UiO-66(Zr) to form electron-rich Pd nanoclusters, which facilitates the production of the desired biaryl product. These studies highlights the great potential of using metal NPs and MOFs for fabricating multifunctional core-shell/core-shell-like structured catalysts for light-induced organic transformations.

On the other hand, some researchers have focused their efforts on the introduction of metal NPs into MOFs shell in order to improve the photocatalytic performances of MOFs catalysts [113,116]. For example, using H<sub>2</sub>PdCl<sub>4</sub> as palladium precursor, Liang et al. [117] successfully synthesized the Pd@MIL-100(Fe) via a facile alcohol reduction approach. In a typical procedure, a mixture of H<sub>2</sub>O (12 mL), ethanol (3 mL), MIL-100(Fe) (100 mg), and a certain amount of H<sub>2</sub>PdCl<sub>4</sub> solution was added into a flask. After the mixed solution was stirred for 15 min, the solid catalysts can be obtained. The complete removal of ibuprofen was achieved in 240 min in Pd@MIL-100(Fe)/H<sub>2</sub>O<sub>2</sub>/Vis system, while only about 54% of ibuprofen was removed in MIL-100(Fe)/H<sub>2</sub>O<sub>2</sub>/Vis system. Besides, Pd@MIL-100(Fe) also showed a better catalytic performance than Pd@Fe<sub>2</sub>O<sub>3</sub> and Pd@TiO<sub>2</sub> under same experimental conditions [117]. This research group also developed a facile photodeposition strategy to fabricate M(M = Au, Pd, Pt)@MIL-100(Fe) nanocomposites [118]. It is reported that M@MIL-100(Fe) solids could be obtained by the visible light irradiation of the mixture of H<sub>2</sub>O (12 mL), ethanol (3 mL), MIL-100(Fe) and metal-ion aqueous solution [118]. The resulting M@MIL-100(Fe) (especially Pd@MIL-100(Fe)) nanocomposites exhibited higher efficiency than MIL-100(Fe) for the photocatalytic degradation of methyl orange (MO) and reduction of Cr(VI) ions. In the both cases, the superior photocatalytic activity of M@MIL-100(Fe) could be ascribed to the more efficient separation of the charge-carrier due to the fact that noble metal NPs can facilitate the interfacial charge transfer [117,118]. As can be seen in Fig. 6a, Pt@MIL-100(Fe) clearly presents the highest photocurrent density among the tested samples, suggesting the most efficient separation of the photogenerated electron-hole pairs. In this M@MIL-100(Fe)/H<sub>2</sub>O<sub>2</sub>/Vis system, the reactive ·OH can be generated via three different pathways

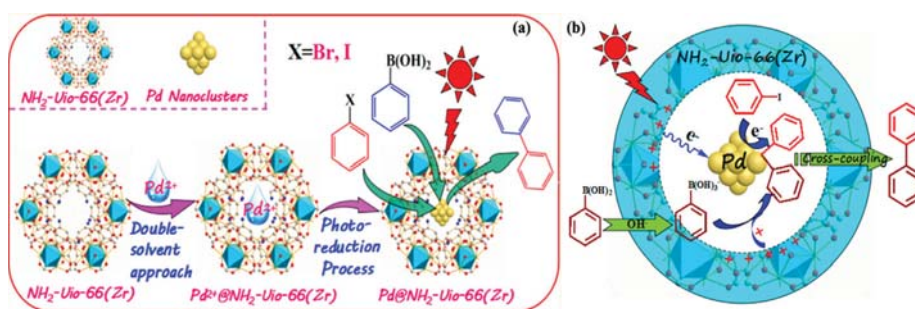


**Fig. 4.** (a) Schematic illustration of the preparation procedures for Pd@NH<sub>2</sub>-Uio-66(Zr); (b) proposed mechanism of the visible-light promoted Suzuki coupling reaction over Pd@NH<sub>2</sub>-Uio-66(Zr). Reproduced with permission from Ref. [112]. Copyright 2016 American Chemical Society.

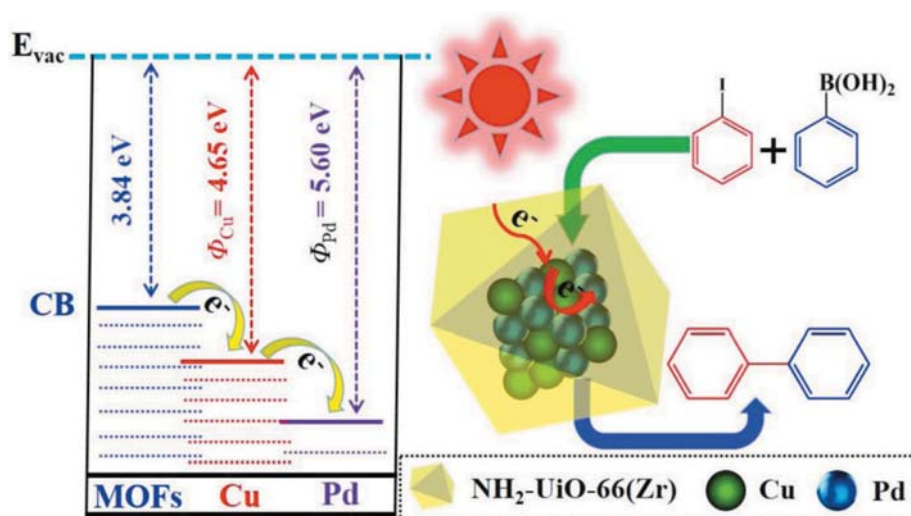


**Fig. 5.** Cu-mediated electron transfer process over CuPd@NH<sub>2</sub>-Uio-66(Zr) for enhanced light-induced Suzuki coupling reaction. Reproduced with permission from Ref. [115]. Copyright 2018 Wiley-VCH.

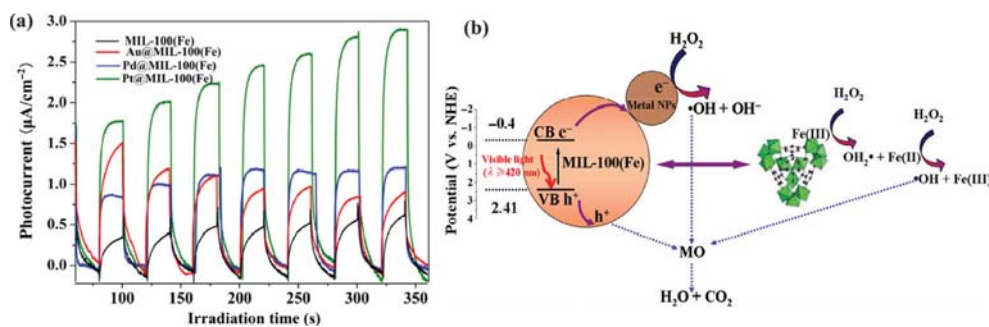


**Fig. 6.** (a) Comparison of transient photocurrent response of MIL-100(Fe) and M (M = Au, Pd, and Pt)@MIL-100(Fe) under intermittent visible-light irradiation ( $\lambda \geq 420$  nm); (b) the proposed mechanism for MO degradation in the M (M = Au, Pd, and Pt)@MIL-100(Fe)/Vis system. Reproduced with permission from Ref. [118]. Copyright 2015 Springer.

(Fig. 6b), namely i) Fenton reaction between H<sub>2</sub>O<sub>2</sub> and Fe(II) species in MIL-100(Fe) (eqs. (16)); ii) H<sub>2</sub>O<sub>2</sub> capturing the photogenerated e<sup>-</sup> to produce  $\cdot\text{OH}$  (eqs. (17)); and iii) the photogenerated h<sup>+</sup> trapping H<sub>2</sub>O to form more  $\cdot\text{OH}$  (Eq. (3)). The enhanced production of reactive  $\cdot\text{OH}$  can thus lead to the high degradation efficiency of organics. In a previous study, Shen and co-workers [119] fabricated a Pd@UiO-66-NH<sub>2</sub> catalyst through the one-pot hydrothermal method. It was demonstrated that the highly dispersed Pd NPs in the MOFs structure can lead to the enhanced light harvesting and more efficient separation of photogenerated electron-hole pairs

(Fig. 7A). As a result, Pd@UiO-66-NH<sub>2</sub> exhibited much higher Cr(VI) reduction ratio (99%) as compared that of UiO-66-NH<sub>2</sub> (38%). Interestingly, it was found that the presence of organic dyes can further increase the photocatalytic reduction efficiency of Cr(VI). This can be ascribed to the consumption of photogenerated h<sup>+</sup> by dyes (Fig. 7B), which decreased the recombination of photoexcited electron-hole pairs.



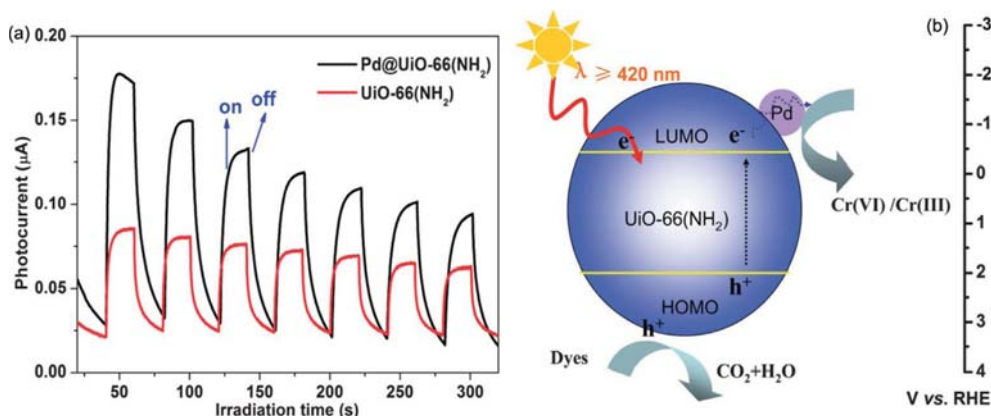


**Fig. 7.** (a) Transient photocurrent response of UiO-66-NH<sub>2</sub> and Pd@UiO-66-NH<sub>2</sub> in 0.2 M Na<sub>2</sub>SO<sub>4</sub> aqueous solution under visible light irradiation; (b) simultaneous photocatalytic degradation of dyes and reduction of Cr(VI) on Pd@UiO-66-NH<sub>2</sub> under visible light irradiation. Reproduced with permission from Ref. [119]. Copyright 2013 The Royal Society of Chemistry.

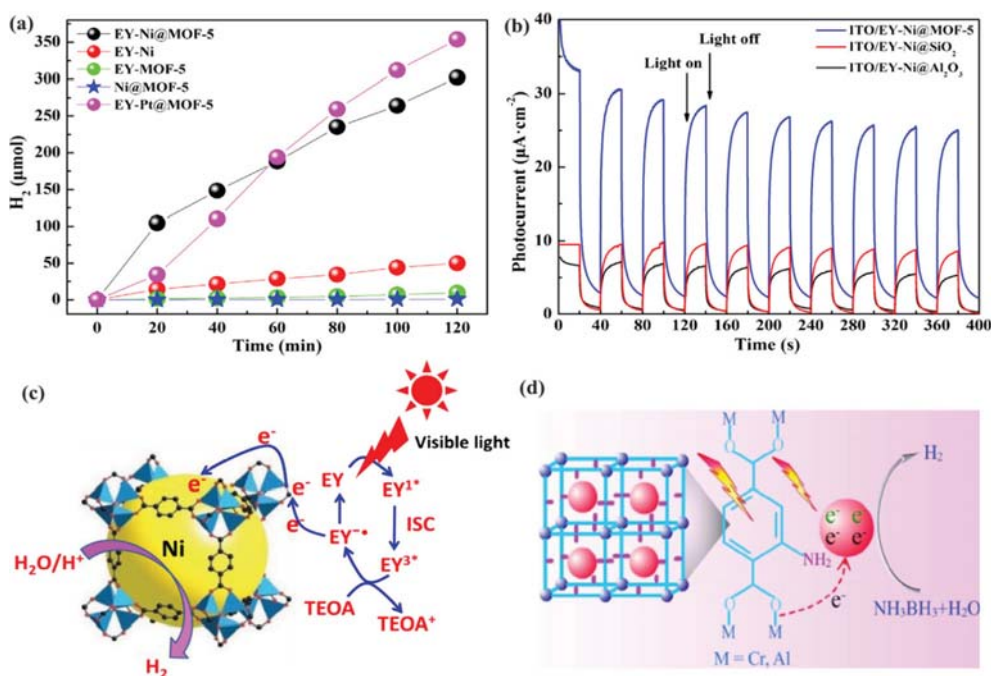


**Fig. 8.** (a) H<sub>2</sub> production in different system. (b) Transient photocurrent response of EY-sensitized Ni, MOF-5, Ni@MOF-5 and Pt@MOF-5 in a mixed solution of Na<sub>2</sub>SO<sub>4</sub> (0.1 mol/L) and 10% (v/v) triethanolamine (TEOA) at pH 11 under intermittent visible light irradiation (≥420 nm). (c) The mechanism for H<sub>2</sub> evolution (TEOA as a sacrificial donor) over the EY sensitized Ni@MOF-5. Reproduced with permission from Ref. [124]. Copyright 2015 Springer. (d) Schematic illustration of the synergistic catalytic H<sub>2</sub> evolution over Ni and Co NPs@NH<sub>2</sub>-functionalized photoactive MOFs from NH<sub>3</sub>BH<sub>3</sub> in aqueous solution under visible light irradiation. Reproduced with permission from Ref. [128]. Copyright 2018 Elsevier.

The non-noble metal nickel (Ni) is a typical active co-catalyst for hydrogen evolution [120–123]. In 2016, Zhen et al. [124] fabricated the Ni@MOF-5 nanocomposites through an impregnation and in situ chemical reduction strategy, and studied its ability to be used as a co-catalyst for visible-light-driven photocatalytic hydrogen evolution. It was reported that 302.2 mol of H<sub>2</sub> can be produced after 2 h reaction using the Eosin Y (EY)-sensitized Ni@MOF-5, which was over 6 times higher than that obtained using Ni particles as the co-catalyst (Fig. 8a). The electrochemical measurements found EY-Ni@MOF-5 exhibited a low overpotential of −0.37 V during the H<sub>2</sub> generation process. This value is comparable to the over-potential of the noble metal contained nanocomposites (Pt@MOF-5) [124]. Such low over-potential of EY-Ni@MOF-5 is resulted from a synergistic effect of small-sized

Ni particles, high specific surface area of MOF-5, and their high dispersion (41.8%) [124]. What's more, it was observed that the overpotential can be reduced by further decrease the diameter of Ni particle. When decreasing the diameter of Ni particle from 9 nm to 3 nm, the over-potential was observed decreased from −0.37 V to −0.35 V accordingly. In addition, the photocatalytic activity of EY-Ni@MOF-5 was found higher than those of EY-Ni@Al<sub>2</sub>O<sub>3</sub> and EY-Ni@SiO<sub>2</sub> (Fig. 8b), which indicated MOF-5 plays a significant role in the photocatalytic H<sub>2</sub> generation. It was suggested that EY can be excited to EY<sup>1\*</sup> state with visible light irradiation, which would subsequently produce a lowest-lying EY<sup>3\*</sup> (the triplet excited state) via an efficient intersystem crossing (Fig. 8c). EY<sup>3\*</sup> could be subsequently quenched by triethanolamine (TEOA, a sacrificial donor), and the produced EY<sup>−</sup> species would then transfer

their  $e^-$  to MOF-5 frameworks because of its electron capture and transport characteristics [125–127]. It is believed that the accumulated  $e^-$  in MOF-5 shells would transfer to the Ni cores, and the protons could finally obtain  $e^-$  from Ni cores to generate  $H_2$  (Fig. 8c). In conclusion, MOF-5 could not only act as an excellent electron acceptor but also the transporter to efficiently prolong the lifetime of photo-generated charge carriers, which consequently improved photocatalytic  $H_2$  evolution activity of EY-Ni@MOF-5. With the same method, in a very recent work [128], a series of M NP@MOF nanocomposites were designed and synthesized by using non-plasmonic Ni and Co NPs and 4 photoactive (MIL-101(Al)-NH<sub>2</sub>, MIL-53(Al)-NH<sub>2</sub>, MIL-101(Cr)-NH<sub>2</sub> and MIL-53(Cr)-NH<sub>2</sub>) or 3 non-photoactive MOFs (MIL-101(Cr), MIL-53(Cr), and MIL-53(Al)). It was found that the nanocomposites containing photoactive MOFs have remarkable higher photocatalytic activities than those containing non-photoactive MOFs, which indicated the 2-aminoterephthalate linkers play a significant role in the catalytic  $H_2$  evolution process. It's worth noting that M NP@photoactive MOFs in this work also exhibited higher total turnover frequency (TOF) values than some previously reported noble metal-containing catalysts such as PdCo NPs [129], AuCo NPs [130] and Pd/SiO<sub>2</sub>-CoFe<sub>2</sub>O<sub>4</sub> [131]. The remarkably enhanced activity was likely caused by the synergistic electron effect of non-plasmonic metal NPs and NH<sub>2</sub>-functionalized photoactive MOFs. As shown in Fig. 8d, on the one hand, the photoactive MOFs can immobilize metal NPs with the NH<sub>2</sub> groups, leading to the effective electron transfer from MOFs to the catalytically active Ni NPs. On the other hand, the NH<sub>2</sub> groups can interact with BH<sub>3</sub> group in NH<sub>3</sub>BH<sub>3</sub>, resulting in the weakened B–H bonds and thus reduced the activation barrier of catalytic  $H_2$  evolution reaction.

## 5. Metal oxide NP@MOF for photocatalysis

Metal oxide catalysts have appeared as essential in most catalytic reactions performed industrially [132–134]. Among various metal oxides with semiconducting properties, TiO<sub>2</sub>, ZnO, and Fe<sub>3</sub>O<sub>4</sub> have received a lot of attention in photocatalysis. TiO<sub>2</sub>, with a bandgap of 3.2 eV, is the most used and classical photocatalytic material [135,136]. TiO<sub>2</sub> has been extensively investigated for decades because of its relatively high photocatalytic activity, nontoxicity, low production cost and its excellent chemical and photochemical stabilities. In the recent years, the application of ZnO in the area of photocatalysis has grown considerably [137–139]. The band-gap energy of ZnO (3.3 eV) is very close to that of TiO<sub>2</sub>, so it theoretically has the similar photocatalytic properties as TiO<sub>2</sub>. In fact, ZnO offers some advantages over TiO<sub>2</sub>, primarily because ZnO is quite strongly luminescent [140]. Fe<sub>3</sub>O<sub>4</sub> has attracted a surge of research interest in photocatalysis especially due to its magnetic properties, which is beneficial for the separation of catalyst from the solution [141,142]. It is well known that the activity of metal oxides in photocatalysis can be enhanced by decreasing their particle size to the nano scale, and thus can lead to the improved catalytic activity per weight unit [132]. However, the practical uses of the metal oxide nanomaterials as photocatalysis have been prevented due to the quick recombination of charge carriers [143]. In the recent years, efforts have been made to develop metal oxides@MOFs nanocomposite as new types of photocatalysts.

### 5.1. TiO<sub>2</sub> NP@MOF

TiO<sub>2</sub>, a widely studied semiconducting photocatalyst, has attracted tremendous attention in the past decades [144–146]. However, it remains challenging to the large-scale industrial application of pure TiO<sub>2</sub> [147–149]. The combination of MOFs and TiO<sub>2</sub>

provides a great opportunity for the construction of new photocatalysts [150]. In 2016, Wang et al. [151] synthesized a semiconductor/MOF nanocomposite (CPO-27-Mg/TiO<sub>2</sub>) for CO<sub>2</sub> reduction via a hydrothermal self-assembly method. Due to its high adsorption capacity toward CO<sub>2</sub> and the existence of open alkaline metal sites in CPO-27-Mg, the as-obtained CPO-27-Mg/TiO<sub>2</sub> nanocomposite exhibited enhanced performance for the photocatalytic CO<sub>2</sub> reduction as compared to the pure CPO-27-Mg and TiO<sub>2</sub> nanospheres. In the recent years, many types of TiO<sub>2</sub>@MOFs core-shell/core-shell like architectures, such as TiO<sub>2</sub>@ZIF-8 [152], TiO<sub>2</sub>@MIL-101(Cr) [153], TiO<sub>2</sub>@NH<sub>2</sub>-MIL-101(Cr) [154], TiO<sub>2</sub>@NH-MIL-125(Ti) [155] and TiO<sub>2</sub>@MIL-100(Fe) [156], have been synthesized and showed enhanced photocatalytic performance. For example, Liu and co-workers [156] developed a sandwich-like hierarchical TiO<sub>2</sub> nanosheets (NS)@MIL-100(Fe) heterostructure by in situ crystal growth of MIL-100(Fe) on TiO<sub>2</sub>NS through a self-assembled strategy (Fig. 9a). The as-synthesized TiO<sub>2</sub>NS@MIL-100(Fe) (Fig. 9b) exhibited the strongest photocurrent intensity (Fig. 9c) and high photocatalytic ability towards methylene blue (MB) under the visible light ( $\geq 420$  nm) radiation, similar results were also reported by some other researchers [153,154,157]. It was suggested that the high number of interfaces in the heterostructures could lead to the enhancement in photocatalytic property by facilitating the separation of electron-hole pairs and accelerating the transfer of photogenerated  $e^-$  [158–160]. As shown in Fig. 9d, photoinduced  $e^-$  can transfer from the CB of MIL-100(Fe) to the CB of TiO<sub>2</sub> NS through the interface reaction between MIL-100(Fe) and TiO<sub>2</sub> NS, which substantially reduces the recombination rate of photo-excited electron-hole pairs and thus improves the photocatalytic activity. As an electron acceptor, H<sub>2</sub>O<sub>2</sub> can produce  $\cdot OH$  over the surface of MIL-100(Fe) [161]. On the other side, the photo-generated holes ( $h^+$ ) in the VB of MIL-100(Fe) simultaneously react with H<sub>2</sub>O to produce  $\cdot OH$  (Fig. 9d).

### 5.2. ZnO NP@MOF

In 2013, Zhan et al. [162] successfully synthesized the free-standing ZnO@ZIF-8 nanorods by a simple self-template strategy for the first time. As shown in Fig. 10A, ZnO nanorods not only provide Zn<sup>2+</sup> ions but also act as the template for the formation of ZIF-8. The TEM images (Fig. 10B) clearly demonstrate that ZnO@ZIF-8 nanorods with the thickness of the outer shell about  $300 \pm 25$  nm have been successfully prepared. Different from the conventional synthetic methods of ZIF-8 [163–166], in this work, no foreign Zn source was required. More importantly, the obtained ZnO@ZIF-8 nanorod arrays exhibited a good photoelectrochemical response to H<sub>2</sub>O<sub>2</sub> (the scavenger). Meanwhile, the photogenerated  $e^-$  can be transferred to the electrode substrate, leading to a remarkable enhancement in the photocurrent response of ZnO nanorods [162]. This study opens a new avenue for fabricating ZnO based photocatalysts. Following this strategy, several research groups have successfully synthesized ZnO@MOF core-shell heterostructures and demonstrated their high catalytic activity for pollutants treatment [167,168], water splitting [169], and liquid hydrogenation [170]. It was suggested that under the light irradiation,  $e^-$  could be more easily excited from the VB to the CB of MOFs in the ZnO@MOF composites [169]. These photo-excited  $e^-$  in the CB of MOFs would be quickly transferred to that of ZnO. In the meantime, the photogenerated  $h^+$  on the VB of ZnO can be transferred to the VB of MOFs shell [171]. The above processes result in more effective separation of photo-excited electron-hole pairs and can thus suppress their recombination [167,169]. More recently, Wang et al. [172] developed an in situ crystal growth strategy for the rapid (within 60 min) fabrication of ZnO@ZIF-8 heterostructures. In this work, 2-methylimidazole (Hmim) was used as the organic ligand. It was reported that the coordination

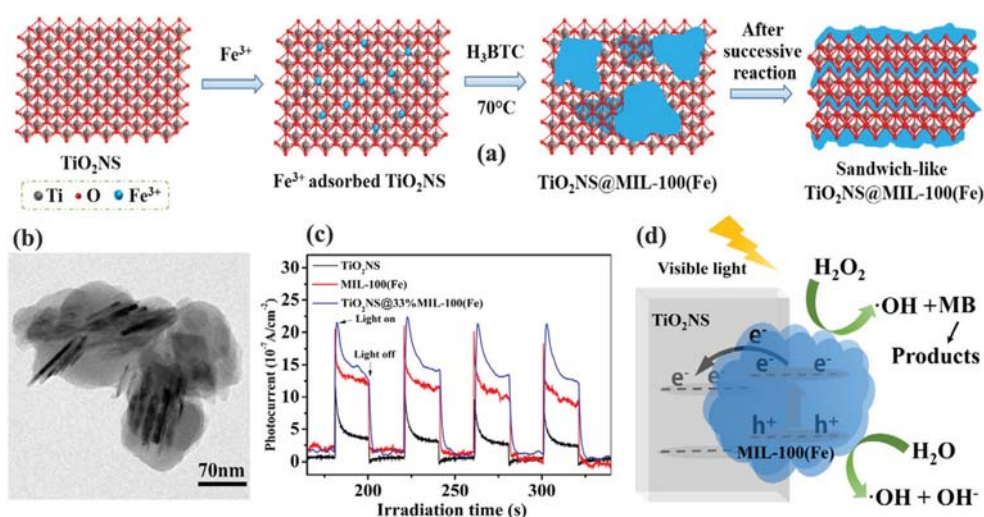


**Fig. 9.** (a) Synthetic illustration of the preparation procedures for TiO<sub>2</sub>NS@MIL-100(Fe). (b) TEM images of the as-synthesized TiO<sub>2</sub>NS@MIL-100(Fe). (c) Transient photocurrent response of MIL-100(Fe), TiO<sub>2</sub>NS, and TiO<sub>2</sub>NS@MIL-100(Fe) in 0.2 M Na<sub>2</sub>SO<sub>4</sub> solution under intermittent visible light irradiation ( $\geq 420$  nm). (d) Proposed mechanism for photocatalytic generation of  $\cdot\text{OH}$  over TiO<sub>2</sub>@MIL-100(Fe). Reproduced with permission from Ref. [156]. Copyright 2017 Elsevier.

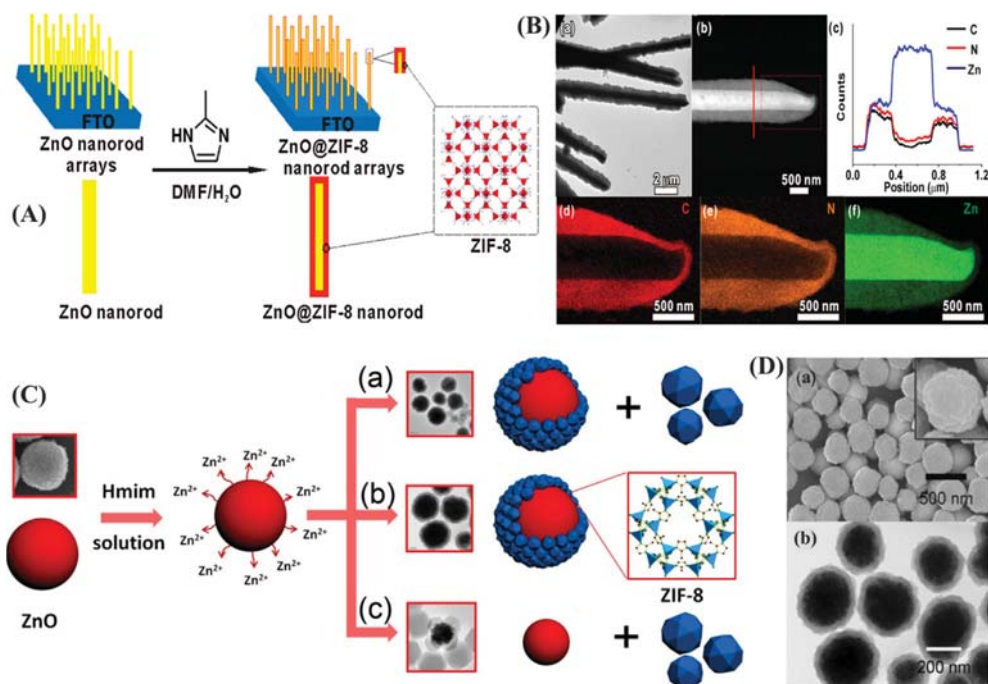


**Fig. 10.** (A) Schematic illustration of the preparation procedures for ZnO@ZIF-8 nanorods. (B) (a) Low-magnification TEM image of ZnO@ZIF-8 nanorods; (b) high-magnification TEM image of an individual ZnO@ZIF-8 nanorod; (c) the cross-sectional compositional line (marked in panel b) profiles of ZnO/ZIF-8; (d–f) the corresponding elemental maps of C, N, and Zn in the ZnO@ZIF-8 nanorod. Reproduced with permission from Ref. [162]. Copyright 2013 American Chemical Society. (C) Schematic illustration of structures obtained using different concentrations of Hmim (a) 4.51 M, (b) 3.66 M, and (c) 1.83 M. (D) SEM (a) and (b) Tem images of ZnO@ZIF-8 heterostructures. Reproduced with permission from Ref. [172]. Copyright 2016 American Chemical Society.

rate of surface bonded Zn<sup>2+</sup> with Hmim is significantly related to the mole ratio of Hmim/Zn<sup>2+</sup>. That's to say, the ideal ZnO@ZIF-8 core-shell heterostructures can be fabricated by controlling the concentration of Hmim (Fig. 10C). Compared with the previous ones (>100 nm of the shell) [162,169], the ZnO@ZIF-8 synthesized by Wang's group has thinner shell (~30 nm, Fig. 10D) and thus has advantages for selective photocatalysis. Their preliminary work demonstrated the as-synthesized ZnO@ZIF-8 could selectively reduce Cr(VI) between Cr(VI) and MB (Fig. 11A), which was believed due to selective permeation effect of ZIF-8 shell (Fig. 11B) [172].

### 5.3. Fe<sub>3</sub>O<sub>4</sub> NP@MOF

In practical applications, MOFs photocatalysts are difficult to be separated from the reaction solution for recycling due to their highly dispersive nature [26,173–176]. Therefore, homogeneous coating of MOFs photocatalysts with magnetic NPs has been put forward to solve this problem [46,177–179]. In 2013, Zhang and co-workers [180] fabricated a novel multifunctional Fe<sub>3</sub>O<sub>4</sub>@MIL-100(Fe) core-shell nanospheres via a versatile layer-by-layer strategy (Fig. 12a). In a typical procedure, the mercaptoacetic acid (MAA)-functionalized Fe<sub>3</sub>O<sub>4</sub> NPs were firstly synthesized by a

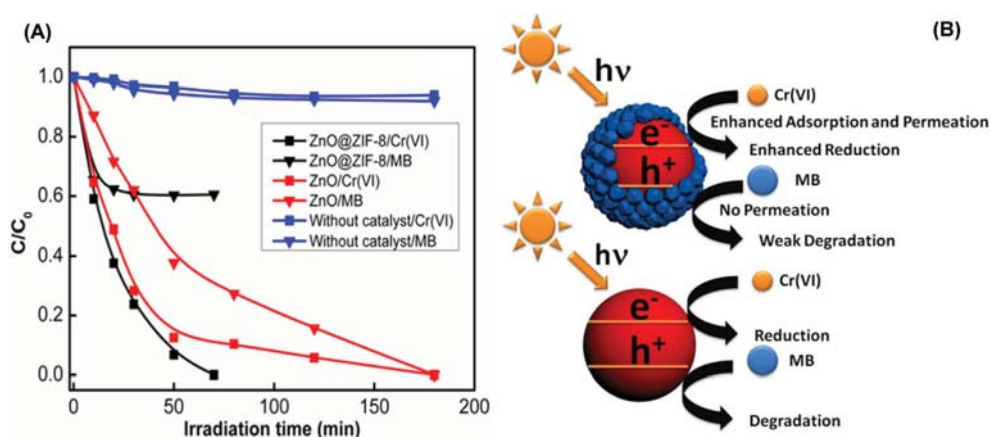


**Fig. 11.** (A) Photocatalytic removal curves of two-component mixed Cr(VI) and MB aqueous solutions. (B) Schematic illustration of selectively enhanced photocatalysis properties of the ZnO@ZIF-8 heterostructures. Reproduced with permission from Ref. [172]. Copyright 2016 American Chemical Society.

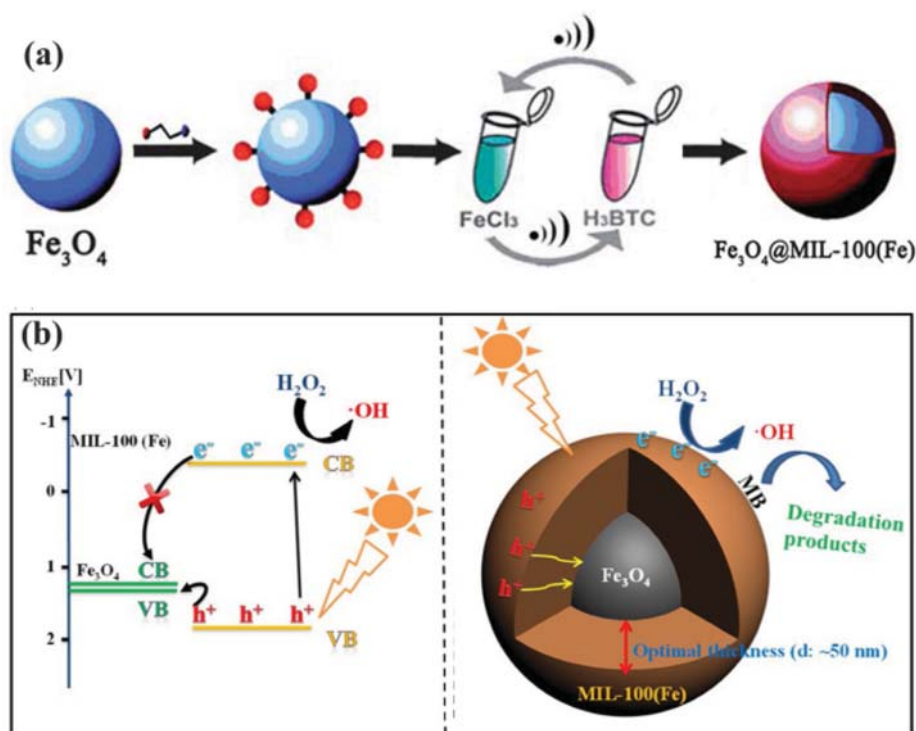


**Fig. 12.** (a) Schematic illustration of the preparation procedures for Fe<sub>3</sub>O<sub>4</sub>@MIL-100(Fe) core-shell microspheres. Reproduced with permission from Ref. [180]. Copyright 2013 The Royal Society of Chemistry. (b) Illustration the possible mechanism for the enhanced photocatalytic ability of Fe<sub>3</sub>O<sub>4</sub>@MIL-100(Fe) with tunable thickness. Reproduced with permission from Ref. [186]. Copyright 2015 Wiley-VCH.

simple stirring process, then the obtained product was fully dispersed in FeCl<sub>3</sub> ethanol solution and subsequently in benzenetricarboxylic acid (H<sub>3</sub>BTC) ethanol solution under ultrasonic conditions, and Fe<sub>3</sub>O<sub>4</sub>@MIL-100(Fe) can be finally obtained after a given number of cycles of the above two procedures. The as-fabricated Fe<sub>3</sub>O<sub>4</sub>@MIL-100(Fe) exhibited remarkable photocatalytic activity for MB degradation, which is higher than those of some typical photocatalysts, such as TiO<sub>2</sub> and C<sub>3</sub>N<sub>4</sub> [180]. It was suggested that MIL-100(Fe) and Fe<sub>3</sub>O<sub>4</sub> present synergistic effect for the generation and transformation of  $e^-$  and  $h^+$  under the light irradiation [181]. As a matter of fact, the magnetic Fe<sub>3</sub>O<sub>4</sub> NPs have also been regarded as a promising photocatalyst due to their wide availability and low toxicity to the environment [182–185]. However, it is well known that Fe<sub>3</sub>O<sub>4</sub> NPs are highly susceptible to photodissolu-

tion, which largely hindered their photocatalytic applications [26]. From this point of view, the Fe<sub>3</sub>O<sub>4</sub>@MOF core-shell structures are desirable also because the exciting radiation could be largely reduced by the MOF shell. Further study demonstrated that the photocatalytic performance of Fe<sub>3</sub>O<sub>4</sub>@MOF nanocomposites is closely related to the thickness of the MOF shell. According to Zhao et al.' work, the shell thickness can be controlled through varying the numbers of assembly cycle, and the optimal shell thickness was determined as about 50 nm [186]. Under light irradiation,  $e^-$  are excited from the VB to the CB of the MIL-100(Fe) shell, leaving  $h^+$  in the VB (Fig. 12b). The generated  $e^-$  can then react with the electron acceptor (H<sub>2</sub>O<sub>2</sub>) to produce  $\cdot\text{OH}$  (Fig. 12b), which is mainly responsible for pollutant degradation [187–189]. In cases where the shell is too small, only a little amount of electron-hole

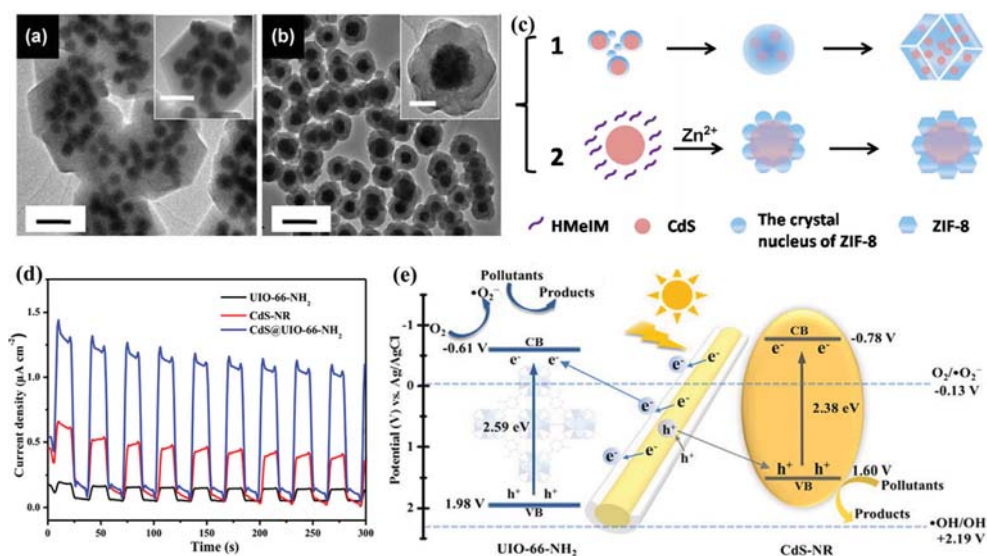


**Fig. 13.** TEM images of MCS (a) and SCS (b) CdS@ZIF-8. The black scale bars in (a) and (b) represent 250 nm, and the white scale bars in (a) and (b) represent 200 and 50 nm, respectively. (c) Schematic illustration of the preparation of MCS (1) and SCS (2) CdS@ZIF-8. Reproduced with permission from Ref. [194]. Copyright 2013 The Royal Society of Chemistry. (d) Transient photocurrent response of the UiO-66-NH<sub>2</sub>, CdS NPs and CdS@UiO-66-NH<sub>2</sub> in 0.2 M Na<sub>2</sub>SO<sub>4</sub> solution under the visible-light irradiation. (e) Proposed mechanism for photocatalytic degradation of pollutants in CdS@UiO-66-NH<sub>2</sub>/Vis system. Reproduced with permission from Ref. [201]. Copyright 2018 Elsevier.

pairs would be generated. If the thickness of MIL-100(Fe) shell thickness is too large, however, the shell-localized holes in MIL-100(Fe) are unable to access the Fe<sub>3</sub>O<sub>4</sub> core, resulting in the charge-carrier recombination, which will inhibit the photocatalytic ability of MIL-100(Fe).

## 6. Other M/MC NP@MOF

Among the visible-light-driven semiconductor photocatalysts, CdS is attracting much attention due to its excellent electronic and optical properties, and suitable band gap (2.4 eV) [190–193]. In 2013, He and co-workers [194] reported the incorporation CdS NPs into MIL-101(Cr) through the post-synthetic method and observed a remarkable enhancement in the photocatalytic H<sub>2</sub> production on CdS. Since then, the incorporation of CdS NPs in many types of MOFs, such as MIL-100(Fe) [195,196] and UiO-66 [197–199], had been put forward as photocatalyst for various applications. In 2016, Zeng et al. [200] described the preparation of well-defined CdS@ZIF-8 nanocomposites by a two-step method. In this work, both multiple-core-shell (MCS) and single-core-shell (SCS) CdS@ZIF-8 (Fig. 13a, b) were fabricated by changing the concentrations of Zn<sup>2+</sup> (Fig. 13c). Compared with pure CdS NPs and SCS CdS@ZIF-8, MCS CdS@ZIF-8 showed higher photocatalytic activity for H<sub>2</sub> generation. More interestingly, the undesired CO generation can be decreased from 12.5% (CdS NPs) to 5.7%, when employing the MCS CdS@ZIF-8 as the catalyst. This is because the size of the narrow windows (3.4 Å) of ZIF-8 is smaller than the kinetic diameter of CO (3.8 Å), thus the generated CO cannot pass through the pores of ZIF-8. As a consequence, the CO generation is suppressed, and the desirable H<sub>2</sub> generation is promoted. Very recently, CdS@MIL-125(Ti) [201] and CdS@UiO-66-NH<sub>2</sub> [202] were developed by the facile one-pot in situ solvothermal approach. In both cases, the core-shell structures produced significant better results than those obtained using single CdS of MOFs. In the first study, the optimized CdS@MIL-125(Ti) sample (with about 8 wt% CdS) showed 2.8 and 1.8 times photoactivity of bulk CdS and MIL-125, respectively [201]. In the second study, the malachite green degradation rate constant of CdS@UiO-66-NH<sub>2</sub> is 27.78 and 4.50 times higher than those of UiO-66-NH<sub>2</sub> and CdS, respec-

tively [202]. The enhanced photoactivity is believed mainly caused by the interface effect between CdS and MOFs, which is able to reduce the recombination rate of photoexcited electron-hole pairs (Fig. 13d) and alleviate the photocorrosion of CdS. As displayed in Fig. 13e, the photo-excited e<sup>-</sup> on the CB of CdS could be transferred to the CB of UiO-66-NH<sub>2</sub>; on the other hand, the h<sup>+</sup> are injected from the VB of MOF to that of CdS, resulting in the effective separation of electron-hole pairs. The h<sup>+</sup> assembled in the CdS core can directly react with the substrate. On the other side, the e<sup>-</sup> on the UiO-66-NH<sub>2</sub> can reduce the dissolved O<sub>2</sub> to produce reactive •O<sub>2</sub><sup>-</sup>, which would then lead to the decomposition of the pollutant.

CdS has been investigated extensively as a photocatalyst for photocatalytic reduction of CO<sub>2</sub>, however, its application has unfortunately been limited due to lack of catalytic sites, the low CO<sub>2</sub> adsorption, and the fast recombination of photogenerated electron-hole pairs [203–206]. It has been demonstrated that the combination of CdS and MOFs can help to overcome their respective shortcomings by facilitating CO<sub>2</sub> adsorption and increasing the visible-light response [207–209]. Recently, Chen et al. [210] synthesized the CdS@UiO-bpy/Co with high stability according the route shown in Fig. 14A. The enhanced light harvesting and more efficient separation of photogenerated electron-hole pairs were observed in CdS@UiO-bpy/Co system (Fig. 14B). Under visible light illumination, the CdS@UiO-bpy/Co composites showed a high CO evolution rate of 235 μmol g<sup>-1</sup> h<sup>-1</sup>, which was about 10 times that of CdS (23 μmol g<sup>-1</sup> h<sup>-1</sup>) under the same conditions. The obtained CO<sub>2</sub> reduction ability of CdS@UiO-bpy/Co composites was comparable to some previously reported catalysts such as MOF-525-Co [211], UiO-66/C<sub>3</sub>N<sub>4</sub> [212] and In<sub>2</sub>S<sub>3</sub>-CdIn<sub>2</sub>S<sub>4</sub> [213]. It was reported that the photocurrent intensity of CdS@UiO-bpy/Co was significantly higher than those of both CdS/UiO-bpy and CdS, suggesting the more effective separation of photoexcited charge carriers in the CdS@UiO-bpy/Co composites. Further studied showed that Co in the CdS@UiO-bpy/Co composites was mainly responsible for the effective transportation of photogenerated e<sup>-</sup> and photoreduction of CO<sub>2</sub> to CO (Fig. 14C).

The combination of silver containing photocatalysts with MOFs has attracted increasing attention [214–217]. For example, Ag<sub>3</sub>-PO<sub>4</sub>@MIL-125-NH<sub>2</sub> nanocomposite has been recently developed based on a one-pot dry-process reaction method [218]. The

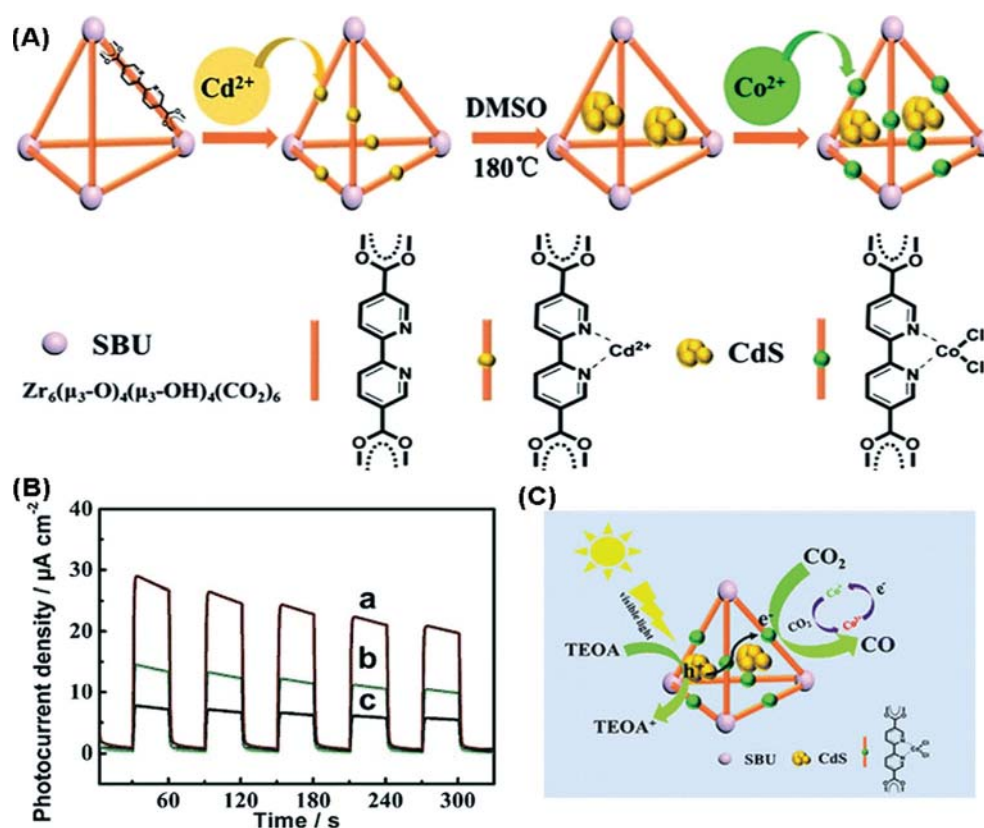


**Fig. 14.** (a) The route for the synthesis of the  $CdS@UiO-bpy/Co$  composites; (B) Transient photocurrent responses under visible light irradiation:  $CdS@UiO-bpy/Co$  (a),  $CdS@UiO-bpy$  (b), and  $CdS$  (c); (C) Proposed mechanism for photocatalytic reduction of  $CO_2$  in  $CdS@UiO-bpy/Co/Vis$  system. Reproduced with permission from Ref. [210]. Copyright 2018 The Royal Society of Chemistry.

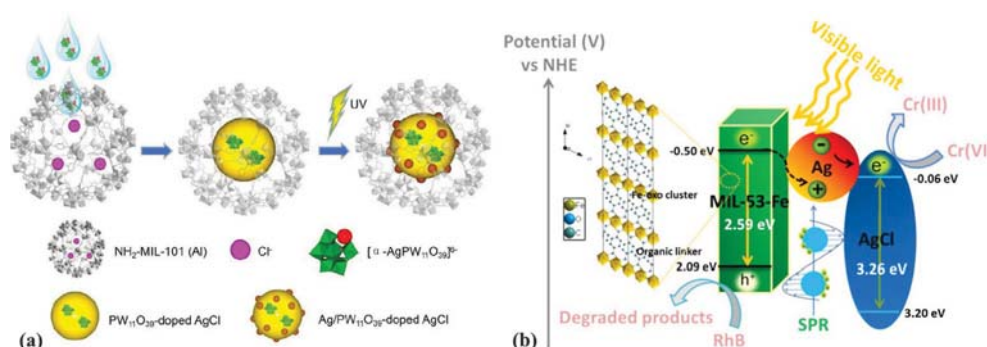


**Fig. 15.** (a) Schematic illustration of the preparation procedures of  $Ag/POMAgCl@NH_2-MIL-101(Al)$ . Reproduced with permission from Ref. [223]. Copyright 2018 Elsevier. (b) Plasmonic Z-scheme photocatalytic mechanism of  $Ag/AgCl@MIL-53-Fe$  under visible light irradiation. Reproduced with permission from Ref. [224]. Copyright 2016 The Royal Society of Chemistry.

$Ag_3PO_4@MIL-125-NH_2$  nanocomposites showed remarkable high photocatalytic activities for MB and rhodamine B (RhB) degradation, which is 39 and 35 times higher than the classical  $TiO_2$  photocatalyst. It was elucidated  $Ag_3PO_4$  NPs played a significant role in lowering the optical band gap of the  $MIL-125-NH_2$ . Specifically, under the light irradiation,  $e^-$  are excited from the VB to the CB of the  $Ag_3PO_4$  and  $MIL-125-NH_2$ , leaving the  $h^+$  in the VB of them. Then, the photo-excited  $e^-/h^+$  can quickly transfer from the CB/VB of  $MIL-125-NH_2$  to those of  $Ag_3PO_4$ , which ensures a long lifetime of photoexcited charge carriers, resulting in higher photocatalytic activity of  $Ag_3PO_4@MIL-125-NH_2$  nanocomposite.  $Ag/AgCl$  NPs has been suggested as a photocatalyst that has a great potential application for the solar light-driven photocatalysis due to the strong surface plasmon resonance (SPR) effect of  $Ag$  NPs [219–222]. In 2016, a novel  $Ag/AgCl@MIL-101(Cr)$  nanocomposite was

fabricated through vapor diffusion of mixtures of  $AgNO_3/MIL-101(Cr)$  solution and a coupled photoreduction strategy [214]. The as-obtained photocatalyst showed an enhanced photoactivity for the degradation of RhB in wastewater under visible light irradiation. In another work, Yan et al. [223] used  $K_6[\alpha-AgPW_{11}O_{39}]$  to control the growth of  $Ag/AgCl$  nanocrystals. It was demonstrated that mono-vacant  $K_6[\alpha-AgPW_{11}O_{39}]$  could act as the stabilizing agent and coordinate with  $Ag^+$ , which can, therefore, tune the reaction speed between  $Ag^+$  and  $Cl^-$ , resulting in the formation of controllable  $AgCl$  nanocrystals. As illustrated in Fig. 15a, the  $Ag-AgCl@MIL-101(Al)-NH_2$  can be obtained via an incipient wetness impregnation combined with the subsequent UV irradiation (photo-reduction) method. The as-obtained nanocomposite exhibited higher photocatalytic activity than  $Ag/AgCl$  and  $Ag/AgCl@MIL-101(Al)-NH_2$  for RhB degradation. Very recently,

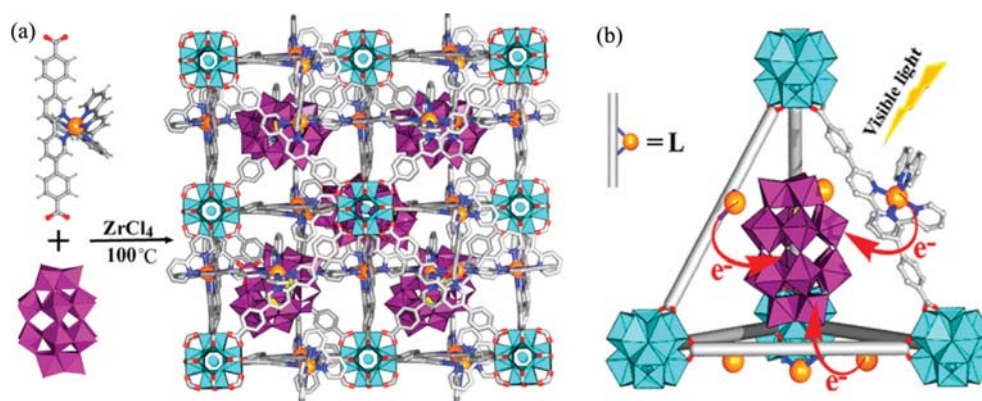


**Fig. 16.** (a) One-pot synthesis of the  $[P_2W_{18}O_{62}]^{6-}$ @UiOs via charge assisted self-assembly.  $[P_2W_{18}O_{62}]^{6-}$ , purple polyhedra; Zr, cyan; Ru, gold; N, blue; O, red; C, light gray. (b) Schematic showing synergistic visible-light excitation of the UiO framework and multielectron injection into the encapsulated POMs. Reproduced with permission from Ref. [229]. Copyright 2015 American Chemical Society.

the Ag/AgCl@MIL-53-Fe hetero-junction photocatalyst was rationally designed and successfully synthesized by using a facile one-pot solvothermal method [224]. It was suggested that plasmonic Z-scheme mechanism in the Ag/AgCl@MIL-53(Fe) can promote the effective separation of photoexcited charge carriers and therefore yielded enhanced photocatalytic activity. As shown in Fig. 15b, the Ag is SPR-excited under light irradiation and the generated  $e^-$  is injected into CB of AgCl, where Cr(VI) could be reduced to Cr(III). The left  $h^+$  in Ag region are simultaneously recombined with the photo-excited  $e^-$  from MIL-53(Fe) to facilitate the separation of charge carrier in MIL-53(Fe), while the  $h^+$  remained on MIL-53(Fe) can directly oxidize RhB.

Polyoxometalates (POMs), a class of discrete nanometric anionic metal oxide clusters, offer huge potential for water-splitting half-reactions due to their ability to undergo fast, stepwise, and reversible multiple electron transfer reactions without changing their structures [225–227]. Several studies have reported the successful synthesis of POM@MOF as efficient photo-catalysts for water-splitting [228–231]. In 2015, Zhang et al. [229] developed a noble POM@MOF ( $[P_2W_{18}O_{62}]^{6-}$ @UiOs) by a simple charge-assisted self-assembly process (Fig. 16a). Under the same conditions, POM@UiOs can produce much more  $H_2$  than  $[P_2W_{18}O_{62}]^{6-}/Me_2L$  and  $[P_2W_{18}O_{62}]^{6-}/[Ru(bpy)_3]Cl_2$ , which can be attributed to the ability of POM@UiOs to undergo facile multielectron injection into each POM encapsulated by six L ligands in the tetrahedral cage (Fig. 16b). In the following years, different types of POM@MOF, including  $Ni_4P_2$ @MOF-1 [232], Co-POM@MIL-101(Cr) [233],  $PW_{12}O_{40}$ @ ZIF-67 [234] and  $P_2W_{18}Co_4$ @MOF-545 [230], have been synthesized and applied for water-splitting. Recently, Paille et al. [230] selected the sandwich-type POM  $[(PW_9O_{34})_2Co_4(H_2O)_2]^{10-}$  (named  $P_2W_{18}Co_4$ ) as the catalytically active guest, and the Zr(IV) porphyrinic MOF-545 as the framework to produce a new POM@MOF (Fig. 17a–d). The immobilization of POM in the pores of MOF was performed by mild aqueous impregnation of MOF-545 with an excess of  $Na_{10}P_2W_{18}Co_4$ . The obtained  $P_2W_{18}Co_4$ @MOF-545 exhibit a high photocatalytic activity for visible-light-driven oxygen evolution from water. The proposed reaction mechanism includes following steps as shown in Fig. 17e: (i) the capture of light by porphyrin in the MOF-545; (ii) one-electron oxidation of the excited state TCPP-MOF\* by the sacrificial electron acceptor ( $Na_2S_2O_8$ ); (iii) one-electron oxidation of POM by TCPP-MOF<sup>+</sup>; and (iv) oxidation of water into  $O_2$ .

## 7. Conclusions and prospects

In this review, we have summarized and exemplified the synthesis of M/MC NP@MOF core-shell and core-shell like nanocom-

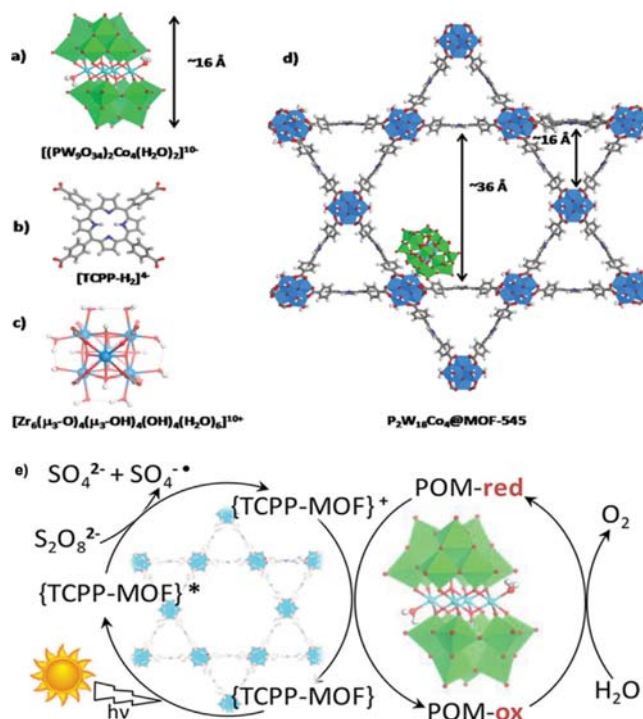


**Fig. 17.** POM@MOF-545 components: (a)  $P_2W_{18}Co_4$  POM; (b) TCPP-H2 linker; (c) Zr-based unit; and (d)  $P_2W_{18}Co_4$ @MOF-545; (e) The proposed mechanism for the light-driven oxygen evolution reaction by  $P_2W_{18}Co_4$ @MOF-545. Reproduced with permission from Ref. [230]. Copyright 2018 American Chemical Society.

posites and their applications in heterogeneous photocatalysis, which includes photocatalytic water-splitting, Cr(VI) reduction,  $CO_2$  reduction, nonselective processes for the degradation of pollutants and selective organic transformations to fine chemicals. Although the application of NP@MOF nanostructures in the field of photocatalysis is still at an early stage, the experimental works have shown the promising potential that exists. Up to now, various synthetic strategies have been developed for incorporation of NPs in MOFs. Generally, the M/MC NP@MOF composites discussed in this review can be classified according to 3 synthetic approaches: (1) the M/MC NPs core and MOFs shell were synthesized simultaneously in a one-pot reaction; (2) the assembly of MOFs precursors on the surface of the pre-synthesized NPs (the 'bottle-around-ship' approach); (3) and the preformed MOFs are introduced into the reaction solution, and the NPs formation within MOFs is

subsequently triggered by the application of light radiation, reducing agents, or heat (the ‘ship-in-a-bottle’ approach). Based on different types of M/MC NPs core and MOFs shell, various kinds of types of M/MC NP@MOF composites have been synthesized and showed enhanced photocatalytic performance.

M/MC NP@MOF composites can combine the respective beneficial characteristics of M/MC NPs and MOFs, in some cases even exhibited unexpected catalytic performance and functions. In particular, the MOFs shell can play one or more of the following roles: (1) stabilize and disperse the NPs; (2) reduce photocorrosion of the M/MC NPs; (3) increase the number of active sites; (4) accumulate the photo-excited electron and transfer to the M/MC NPs; (5) transfer reaction substrates to the M/MC NPs surface; (6) enable the size-selective catalysis of target substrates. In turn, the M/MC NPs endow the MOFs with desirable light-harvesting capability or optoelectronic property. Taking together, the combination of M/MC NPs and MOFs can facilitate the interfacial charge transfer and reduce the recombination rate of photogenerated electron-hole pairs, leading to the enhanced photocatalytic performance.

Due to the outstanding advantages of M/MC NP@MOF core-shell nanocomposites, such as multifunctional cores and shells, and tunable pore sizes of the shells, they will provide an unprecedented opportunity for the development of alternative photocatalysts. However, despite that great achievements have been made in NP@MOF core-shell nanocomposites design and synthesis, many more efforts need to be done before these catalysts can be industrially produced and applied.

1) Most research in this research field is still at the lab-scale stage, in which only a small amount of catalysts were synthesized. What's more, some of these synthetic methods are complex and difficult to control. Therefore, the development of more facile synthetic methods (especially the one-step synthesis methods) which can be applied for large-scale production is highly desirable.

2) There remain some challenges regarding the synthesis of M/MC NP@MOF photocatalysts, in particular using the ‘ship-in-a-bottle’ approach where precise control over the location together with the size of the NPs is especially difficult. As for the ‘bottle-a-round-ship’ approach, how to realize controllable growth (e.g., the structure and thickness) of MOFs on the surface of NPs while keeping the dispersibility, shape and size of M/MC NPs will be one of the key research topics in the future. The development of novel in situ encapsulation strategies that would enable tuning of the sizes, shapes, composition, and uniformity of the obtained hybrid composites is highly desirable.

3) The types of M/MC NPs in the nanocomposites should be extended. In particular, to date, most studies in this field have been conducted with semiconductor as the core material. Research into the encapsulation of noble metal NPs in MOFs for photocatalysis is rare, even though noble metal NPs show very promising catalysis. Besides, many base metals have presented significant potential in catalyzing a wide range of organic reactions. To expand the application scope, more attention should be devoted in the future to investigating the encapsulation of noble metal NPs, base metals NPs and other functional NPs in MOFs.

4) The highly tailorable pore environments in MOFs play vital roles in regulating the catalytic behavior of the M/MC NP@MOF nanocomposites and have great potential in catalysis, which, however, is far from being well developed. For example, the design of selective catalyst through controlling the pore size, organic linkers or hydrophobicity of the MOFs shell is certainly interesting and should be further explored.

5) The detailed structure of many types of M/MC NP@MOF nanocomposites is unclear, which largely impedes the clarification of structure-catalysis relationships. Therefore, theoretical calculations on a NP@MOF composite with a precise structure would be urgently desired.

6) A fundamental in-depth understanding of many factors, such as the size and shape of the core, the thickness, porosity and hydrophobicity of the shell, on the photocatalytic performance needs to be further explored, which is vital for the design of smarter M/MC NP@MOF core-shell catalysts for target applications. It is worth mentioning that several researchers have found the shell thickness can significantly alter the catalytic performance of M/MC NP@MOF catalysts. These pioneering works point out a new way to promote the catalytic activity of M/MC NP@MOF catalysts.

7) In order to meet the practical requirements, more efforts are needed to gain a better understanding of the M/MC NP@MOF photocatalysts, such as the photocatalytic selectivity in solutions containing more components, the chemical stability of these catalysts during the circular process in different pH solutions at different temperatures, etc. Besides, the environmental risk assessment of these nanostructure photocatalysts should be adequately conducted before practical applications. Particularly, for the pollutants degradation applications, the toxicity of intermediate products needs to be carefully evaluated since photocatalytic degradation often fails to completely mineralize the pollutants.

8) Many issues related to the mechanisms need more investigations. For example, it is necessary to recognize the roles of both components and understand how they synergize to achieve high catalytic activity. The better understanding of the structure-activity relationship may pave a way for rational design of excellent M/MC NP@MOF photocatalysts and provide a guide for uncovering the behind photocatalytic mechanisms.

9) Last but not least, progress in the field of M/MC NP@MOF photocatalysts cannot be independent of research on MOFs. The development of new types of MOFs with excellent photocatalytic activity, tailorable pore environments, high stability and recyclability is still urgently required for the rational design of M/MC NP@MOF photocatalysts.

## Acknowledgements

This study was financially supported by the Program for the National Natural Science Foundation of China (51579098, 51521006, 51779090, 51679085), the National Program for Support of Top-Notch Young Professionals of China (2014), the Program for Changjiang Scholars and Innovative Research Team in University (IRT-13R17), the Program for New Century Excellent Talents in University (NCET-13-0186), China Postdoctoral Science Foundation Funded Project (2018M642977), Hunan Provincial Science and Technology Plan Project (2018SK20410, 2017SK2243, 2016RS3026), and the Fundamental Research Funds for the Central Universities (531109200027, 531107051080, 531107050978, 531107051205).

## References

- [1] A.T. Bell, *Science* 299 (2003) 1688–1691.
- [2] M. Yoon, R. Srirambalaji, K. Kim, *Chem. Rev.* 112 (2012) 1196–1231.
- [3] A. Corma, H. García, F.X. Llabrés i Xamena, *Chem. Rev.* 41 (2010) 4606–4655.
- [4] B. Li, C. Lai, G. Zeng, L. Qin, H. Yi, D. Huang, C. Zhou, X. Liu, M. Cheng, P. Xu, C. Zhang, F. Huang, S. Liu, *ACS Appl. Mater. Interfaces* 10 (2018) 18824–18836.
- [5] R. Asahi, T. Morikawa, T. Ohwaki, K. Aoki, Y. Taga, *Science* 293 (2001) 269–271.
- [6] X. Lang, X. Chen, J. Zhao, *Chem. Soc. Rev.* 43 (2013) 473–486.
- [7] M.-H. Sun, S.-Z. Huang, L.-H. Chen, Y. Li, X.-Y. Yang, Z.-Y. Yuan, B.-L. Su, *Chem. Soc. Rev.* 45 (2016) 3479–3563.
- [8] C. Zhou, C. Lai, D. Huang, G. Zeng, C. Zhang, M. Cheng, L. Hu, J. Wan, W. Xiong, M. Wen, X. Wen, L. Qin, *Appl. Catal. B: Environ.* 220 (2018) 202–210.
- [9] C. Zhou, C. Lai, P. Xu, G. Zeng, D. Huang, C. Zhang, M. Cheng, L. Hu, J. Wan, Y. Liu, W. Xiong, Y. Deng, M. Wen, *ACS Sustainable Chem. Eng.* 6 (2018) 4174–4184.
- [10] J. Schneider, M. Matsuoka, M. Takeuchi, J. Zhang, Y. Horiuchi, M. Anpo, D.W. Bahnemann, *Chem. Rev.* 114 (2014) 9919–9986.
- [11] C. Lai, M.M. Wang, G.M. Zeng, Y.G. Liu, D.L. Huang, C. Zhang, R.Z. Wang, P. Xu, M. Cheng, C. Huang, *Appl. Surf. Sci.* 390 (2016) 368–376.

- [12] X. Zhou, C. Lai, D. Huang, G. Zeng, L. Chen, L. Qin, P. Xu, M. Cheng, C. Huang, C. Zhang, *J. Hazard. Mater.* 346 (2018) 113.
- [13] Z. Zhang, J. Jiatieli, D. Liu, F. Yu, S. Xue, W. Gao, Y. Li, D.D. Dionysiou, *Chem. Eng. J.* 231 (2013) 84–93.
- [14] Y. Zhang, C. Han, G. Zhang, D.D. Dionysiou, M.N. Nadagouda, *Chem. Eng. J.* 268 (2015) 170–179.
- [15] Y. Zhang, C. Han, M.N. Nadagouda, D.D. Dionysiou, *Appl. Catal. B: Environ.* 168–169 (2015) 550–558.
- [16] T. Zhang, W. Lin, *Chem. Soc. Rev.* 43 (2014) 5982–5993.
- [17] N.L. Rosi, J. Eckert, M. Eddaoudi, D.T. Vodak, J. Kim, M. O’Keeffe, O.M. Yaghi, *Science* 300 (2003) 1127–1129.
- [18] H. Furukawa, K.E. Cordova, M. O’Keeffe, O.M. Yaghi, *Science* 341 (2013) 1230444.
- [19] J.R. Long, O.M. Yaghi, *Chem. Soc. Rev.* 38 (2009) 1213.
- [20] W. Xiong, Z. Zeng, X. Li, G. Zeng, R. Xiao, Z. Yang, Y. Zhou, C. Zhang, M. Cheng, L. Hu, C. Zhou, L. Qin, R. Xu, Y. Zhang, *Chemosphere* 210 (2018) 1061–1069.
- [21] X. Wang, W. Chen, L. Zhang, T. Yao, W. Liu, Y. Lin, H. Ju, J. Dong, L. Zheng, W. Yan, X. Zheng, Z. Li, X. Wang, J. Yang, D. He, Y. Wang, Z. Deng, Y. Wu, Y. Li, *JACS* 139 (2017) 9419–9422.
- [22] X. Lin, J. Jia, P. Hubberstey, M. Schröder, N.R. Champness, *Crystengcomm* 9 (2007) 438–448.
- [23] G. Lu, J.T. Hupp, *JACS* 132 (2010) 7832.
- [24] W. Xiong, G. Zeng, Z. Yang, Y. Zhou, C. Zhang, M. Cheng, Y. Liu, L. Hu, J. Wan, C. Zhou, R. Xu, X. Li, *Sci. Total Environ.* 627 (2018) 235–244.
- [25] P. Horcajada, C. Serre, M. ValletínEgi, M. Sebban, F. Taulelle, G. Férey, *Angew. Chem. Int. Ed.* 45 (2010) 5974–5978.
- [26] M. Cheng, C. Lai, Y. Liu, G. Zeng, D. Huang, C. Zhang, L. Qin, L. Hu, C. Zhou, W. Xiong, *Coord. Chem. Rev.* 368 (2018) 80–92.
- [27] X. Deng, Z. Li, H. García, *Chem. A Eur. J.* 23 (2017) 11189–11209.
- [28] Zhengde Dai, Jun Liu, Dongling Li, *Chem. Soc. Rev.* 45 (2015) 6011–6061.
- [29] A.H. Chughtai, N. Ahmad, H.A. Younus, A. Laypkov, F. Verpoort, *Chem. Soc. Rev.* 44 (2015) 6804–6849.
- [30] B. Shao, Z. Liu, G. Zeng, Y. Liu, X. Yang, C. Zhou, M. Chen, Y. Liu, Y. Jiang, M. Yan, *J. Hazard. Mater.* 362 (2019) 318–326.
- [31] A. Dhakshinamoorthy, Z. Li, H. García, *Chem. Soc. Rev.* 47 (2018) 8134–8172.
- [32] Y. Chen, D. Wang, X. Deng, Z. Li, *Catal. Sci. Technol.* 7 (2017) 4893–4904.
- [33] D. Sun, Z. Li, Chin. *J. Chem.* 35 (2017) 135–147.
- [34] X. Deng, M. Hao, Z. Li, *Curr. Org. Chem.* 22 (2018) 1825–1835.
- [35] F.X.L.I. Xamena, A. Corma, H. García, *J. Phys. Chem. C* 111 (2007) 80–85.
- [36] S. Wang, X. Wang, *Small* 11 (2015) 3097–3112.
- [37] C.C. Wang, J.R. Li, X.L. Lv, Y.Q. Zhang, G. Guo, *Energy Environ. Sci.* 7 (2014) 2831–2867.
- [38] A. Dhakshinamoorthy, A.M. Asiri, H. García, *Angew. Chem. Int. Ed.* 55 (2016) 5414–5445.
- [39] Z. Liang, C. Qu, D. Xia, R. Zou, Q. Xu, *Angew. Chem. Int. Ed.* 57 (2018) 9604–9633.
- [40] M. Cheng, Y. Liu, D. Huang, C. Lai, G. Zeng, J. Huang, Z. Liu, C. Zhang, C. Zhou, L. Qin, W. Xiong, H. Yi, Y. Yang, *Chem. Eng. J.* 362 (2019) 865–876.
- [41] R. Liang, F. Jing, L. Shen, N. Qin, L. Wu, J. Hazard. Mater. 287 (2015) 364–372.
- [42] F. Jing, R. Liang, J. Xiong, R. Chen, S. Zhang, Y. Li, L. Wu, *Appl. Catal. B: Environ.* 206 (2017) 9–15.
- [43] F. Zhang, Y. Jin, J. Shi, Y. Zhong, W. Zhu, M.S. El-Shall, *Chem. Eng. J.* 269 (2015) 236–244.
- [44] G. Maurin, C. Serre, A. Cooper, G. Férey, *Chem. Soc. Rev.* 46 (2017) 3104–3107.
- [45] D. Wang, Z. Li, *Res. Chem. Intermed.* 43 (2017) 5169–5186.
- [46] P. Falcaro, R. Ricco, A. Yazdi, I. Imaz, S. Furukawa, D. Maspoch, R. Ameloot, J.D. Evans, C.J. Doonan, *Coord. Chem. Rev.* 307 (2016) 237–254.
- [47] A. Zanon, F. Verpoort, *Coord. Chem. Rev.* 353 (2017) 201–222.
- [48] Z. Li, M. Li, Z. Bian, Y. Kathiraser, S. Kawi, *Appl. Catal. B: Environ.* 188 (2016) 324–341.
- [49] Y. Liu, Z. Tang, *Adv. Mater.* 25 (2013) 5819–5825.
- [50] Q.-L. Zhu, Q. Xu, *Chem. Soc. Rev.* 43 (2014) 5468–5512.
- [51] P. Hu, J.V. Morabito, C.-K. Tsung, *ACS Catal.* 4 (2014) 4409–4419.
- [52] G. Huang, Q. Yang, Q. Xu, S.H. Yu, H.L. Jiang, *Angew. Chem. Int. Ed.* 55 (2016) 7379–7383.
- [53] N. Zhang, S. Liu, Y.-J. Xu, *Nanoscale* 4 (2012) 2227–2238.
- [54] J. Qiu, X. Zhang, Y. Feng, X. Zhang, H. Wang, J. Yao, *Appl. Catal. B: Environ.* 231 (2018).
- [55] Q. Yang, Q. Xu, H.L. Jiang, *Chem. Soc. Rev.* 46 (2017) 4774.
- [56] D. Jiang, P. Xu, H. Wang, G. Zeng, D. Huang, M. Chen, C. Lai, C. Zhang, J. Wan, W. Xue, *Coord. Chem. Rev.* 376 (2018) 449–466.
- [57] J. Wen, X. Li, W. Liu, Y. Fang, J. Xie, Y. Xu, *Chin. J. Catal.* 36 (2015) 2049–2070.
- [58] A.J. Bard, *Science* 207 (1980) 139–144.
- [59] Y. Yang, Z. Zeng, C. Zhang, D. Huang, G. Zeng, R. Xiao, C. Lai, C. Zhou, H. Guo, W. Xue, M. Cheng, W. Wang, J. Wang, *Chem. Eng. J.* 349 (2018) 808–821.
- [60] W. Wang, P. Xu, M. Chen, G. Zeng, C. Zhang, C. Zhou, Y. Yang, D. Huang, C. Lai, M. Cheng, L. Hu, W. Xiong, H. Guo, M. Zhou, *ACS Sustainable Chem. Eng.* 6 (2018) 15503–15516.
- [61] A.B. Djurišić, Y.H. Leung, A.M. Ching Ng, *Mater. Horiz.* 1 (2014) 400–410.
- [62] X. Li, J. Yu, M. Jaronic, *Chem. Soc. Rev.* 45 (2016) 2603–2636.
- [63] D. Huang, C. Hu, G. Zeng, M. Cheng, P. Xu, X. Gong, R. Wang, W. Xue, *Sci. Total Environ.* 574 (2017) 1599–1610.
- [64] W. Xue, D. Huang, G. Zeng, J. Wan, C. Zhang, R. Xu, M. Cheng, R. Deng, J. Hazard. Mater. 341 (2018) 381–389.
- [65] A. Kudo, Y. Miseki, *Chem. Soc. Rev.* 38 (2009) 253–278.
- [66] X. Chen, S. Shen, L. Guo, S.S. Mao, *Chem. Rev.* 110 (2010) 6503.
- [67] X. Gong, D. Huang, Y. Liu, G. Zeng, R. Wang, J. Wan, C. Zhang, M. Cheng, X. Qin, W. Xue, *Environ. Sci. Technol.* 51 (2017) 11308–11316.
- [68] J. Low, B. Cheng, J. Yu, *Appl. Surf. Sci.* 392 (2017) 658–686.
- [69] Z.-H. Yan, M.-H. Du, J. Liu, S. Jin, C. Wang, G.-L. Zhuang, X.-J. Kong, L.-S. Long, L.-S. Zheng, *Nat. Commun.* 9 (2018) 3353.
- [70] Y. Wang, N.-Y. Huang, J.-Q. Shen, P.-Q. Liao, X.-M. Chen, J.-P. Zhang, *JACS* 140 (2018) 38–41.
- [71] X. Wang, Z. Chen, X. Zhao, T. Yao, W. Chen, R. You, C. Zhao, G. Wu, J. Wang, W. Huang, J. Yang, X. Hong, S. Wei, Y. Wu, Y. Li, *Angew. Chem.* 130 (2018) 1962–1966.
- [72] I.I. Alkhatib, C. Garlisi, M. Pagliaro, K. Al-Ali, G. Palmisano, *Catal. Today* (2018).
- [73] L. Chen, R. Luque, Y. Li, *Chem. Soc. Rev.* 46 (2017) 4614–4630.
- [74] G. Li, S. Zhao, Y. Zhang, Z. Tang, *Adv. Mater.* 30 (2018) 1800702.
- [75] W. Xiang, Y. Zhang, H. Lin, C.-J. Liu, *Molecules* 22 (2017) 2103.
- [76] A. Aijaz, A. Karkamkar, Y.J. Choi, N. Tsumori, E. Rönnebro, T. Autrey, H. Shioyama, Q. Xu, *JACS* 134 (2012) 13926–13929.
- [77] Q.-L. Zhu, J. Li, Q. Xu, *JACS* 135 (2013) 10210–10213.
- [78] W. Zhen, F. Gao, B. Tian, P. Ding, Y. Deng, Z. Li, H. Gao, G. Lu, *J. Catal.* 348 (2017) 200–211.
- [79] L. Qin, G. Zeng, C. Lai, D. Huang, P. Xu, C. Zhang, M. Cheng, X. Liu, S. Liu, B. Li, H. Yi, *Coord. Chem. Rev.* 359 (2018) 1–31.
- [80] X. Wang, W. Wang, M. Qiao, G. Wu, W. Chen, T. Yuan, Q. Xu, M. Chen, Y. Zhang, X. Wang, J. Wang, J. Ge, X. Hong, Y. Li, Y. Wu, Y. Li, *Sci. Bull.* 63 (2018) 1246–1253.
- [81] Y. Qu, Z. Li, W. Chen, Y. Lin, T. Yuan, Z. Yang, C. Zhao, J. Wang, C. Zhao, X. Wang, F. Zhou, Z. Zhuang, Y. Wu, Y. Li, *Nat. Catal.* 1 (2018) 781–786.
- [82] J. Yang, Z. Qiu, C. Zhao, W. Wei, W. Chen, Z. Li, Y. Qu, J. Dong, J. Luo, Z. Li, Y. Wu, *Angew. Chem. Int. Ed.* 57 (2018) 14095–14100.
- [83] J. Liu, L. Chen, H. Cui, J. Zhang, L. Zhang, C.-Y. Su, *Chem. Soc. Rev.* 43 (2014) 6011–6061.
- [84] A. Kolmakov, D.O. Klenov, Y. Lilach, S. Stemmer, M. Moskovits, *Nano Lett.* 5 (2005) 667–673.
- [85] X. Zou, Y. Zhang, *Chem. Soc. Rev.* 44 (2015) 5148–5180.
- [86] J. Yang, B. Chen, X. Liu, W. Liu, Z. Li, J. Dong, W. Chen, W. Yan, T. Yao, X. Duan, Y. Wu, Y. Li, *Angew. Chem. Int. Ed.* (2018) 9495–9500.
- [87] P. Yin, T. Yao, Y. Wu, L. Zheng, Y. Lin, W. Liu, H. Ju, J. Zhu, X. Hong, Z. Deng, G. Zhou, S. Wei, Y. Li, *Angew. Chem. Int. Ed.* 55 (2016) 10800–10805.
- [88] P.V. Kamat, *J. Phys. Chem. Lett.* 1 (2010) 520–527.
- [89] M.B. Gawande, A. Goswami, F.-X. Felpin, T. Asefa, X. Huang, R. Silva, X. Zou, R. Zboril, R.S. Varma, *Chem. Rev.* 116 (2016) 3722–3811.
- [90] Y. Hu, J.O. Jensen, W. Zhang, L.N. Cleemann, W. Xing, N.J. Bjerrum, Q. Li, *Angew. Chem. Int. Ed.* 53 (2014) 3675–3679.
- [91] G.-H. Wang, J. Hilgert, F.H. Richter, F. Wang, H.-J. Bongard, B. Spliethoff, C. Weidenthaler, F. Schueth, *Nat. Mater.* 13 (2014) 294–301.
- [92] E. Yoo, T. Okata, T. Akita, M. Kohyama, J. Nakamura, I. Honma, *Nano Lett.* 9 (2009) 2255–2259.
- [93] S. Sakhivel, M.V. Shankar, M. Palanichamy, B. Arabindoo, D.W. Bahnemann, V. Murugesan, *Water Res.* 38 (2004) 3001–3008.
- [94] D. Wang, Y. Song, J. Cai, L. Wu, Z. Li, *New J. Chem.* 40 (2016) 9170–9175.
- [95] M. Cheng, G. Zeng, D. Huang, C. Lai, Y. Liu, C. Zhang, R. Wang, L. Qin, W. Xue, B. Song, S. Ye, H. Yi, *J. Colloid Interface Sci.* 515 (2018) 232–239.
- [96] B. Wang, Z. Deng, X. Fu, C. Xu, Z. Li, *Appl. Catal. B: Environ.* 237 (2018) 970–975.
- [97] C. Zhang, W. Wang, A. Duan, G. Zeng, D. Huang, C. Lai, X. Tan, M. Cheng, R. Wang, C. Zhou, *Chemosphere* 222 (2019) 184–194.
- [98] M. Zhao, K. Deng, L. He, Y. Liu, G. Li, H. Zhao, Z. Tang, *JACS* 136 (2014) 1738–1741.
- [99] L. Chen, Y. Peng, H. Wang, Z. Gu, C. Duan, *Chem. Commun.* 50 (2014) 8651–8654.
- [100] H. Wang, L. Chen, Y. Feng, H. Chen, *Acc. Chem. Res.* 46 (2013) 1636–1646.
- [101] H. Sun, J. He, J. Wang, S.-Y. Zhang, C. Liu, T. Sritharan, S. Mhaisalkar, M.-Y. Han, D. Wang, H. Chen, *JACS* 135 (2013) 9099–9110.
- [102] G. Li, Z. Tang, *Nanoscale* 6 (2014) 3995–4011.
- [103] R. Liu, S.M. Mahurin, C. Li, R.R. Unocic, J.C. Idrobo, H. Gao, S.J. Pennycook, S. Dai, *Angew. Chem. Int. Ed.* 50 (2011) 6799–6802.
- [104] A. Guerrero-Martínez, J. Pérez-Juste, L.M. Liz-Marzán, *Adv. Mater.* 22 (2010) 1182–1195.
- [105] Q. Yang, Q. Xu, S.-H. Yu, H.-L. Jiang, *Angew. Chem.* 128 (2016) 3749–3753.
- [106] L. Lin, H. Liu, X. Zhang, *Appl. Surf. Sci.* 433 (2018) 602–609.
- [107] C.H. Kuo, Y. Tang, L.Y. Chou, B.T. Sneed, C.N. Brodsky, Z. Zhao, C.K. Tsung, *JACS* 134 (2012) 14345.
- [108] X. Yang, S. Yuan, L. Zou, H. Drake, Y. Zhang, J. Qin, A. Alsalmeh, H. Zhou, *Angew. Chem. Int. Ed.* 57 (2018) 3927–3932.
- [109] L. Lin, T. Zhang, H. Liu, J. Qiu, X. Zhang, *Nanoscale* 7 (2015) 7615.
- [110] H. Bux, A. Feldhoff, J. Cravillon, M. Wiebcke, Y.S. Li, J. Caro, *Chem. Mater.* 23 (2011) 2262–2269.
- [111] L. Chang, Y. Li, *Mol. Catal.* 433 (2017) 77–83.
- [112] D. Sun, Z. Li, *J. Phys. Chem. C* 120 (2016) 19744–19750.
- [113] D. Wang, Z. Li, *J. Catal.* 342 (2016) 151–157.
- [114] D. Wang, Y. Pan, L. Xu, Z. Li, *J. Catal.* 361 (2018) 248–254.
- [115] D. Sun, M. Xu, Y. Jiang, J. Long, Z. Li, *Small Methods* 2 (2018) 1800164.
- [116] C. Hou, Q. Xu, Y. Wang, X. Hu, *RSC Adv.* 3 (2013) 19820–19823.
- [117] R. Liang, S. Luo, F. Jing, L. Shen, N. Qin, L. Wu, *Appl. Catal. B: Environ.* 176–177 (2015) 240–248.
- [118] R. Liang, F. Jing, L. Shen, N. Qin, L. Wu, *Nano Res.* 8 (2015) 3237–3249.
- [119] L. Shen, W. Wu, R. Liang, R. Lin, L. Wu, *Nanoscale* 5 (2013) 9374–9382.

- [120] D. Kong, J.J. Cha, H. Wang, H.R. Lee, Y. Cui, *Energy Environ. Sci.* 6 (2013) 3553–3558.
- [121] M.L. Helm, M.P. Stewart, R.M. Bullock, M.R. DuBois, D.L. DuBois, *Science* 333 (2011) 863–866.
- [122] M. Gong, W. Zhou, M.-C. Tsai, J. Zhou, M. Guan, M.-C. Lin, B. Zhang, Y. Hu, D.-Y. Wang, J. Yang, S.J. Pennycook, B.-J. Hwang, H. Dai, *Nat. Commun.* 5 (2014) 4695.
- [123] W.-F. Chen, K. Sasaki, C. Ma, A.I. Frenkel, N. Marinkovic, J.T. Muckerman, Y. Zhu, R.R. Adzic, *Angew. Chem. Int. Ed.* 51 (2012) 6131–6135.
- [124] W. Zhen, J. Ma, G. Lu, *Appl. Catal. B: Environ.* 190 (2016) 12–25.
- [125] W. Zhang, J. Hong, J. Zheng, Z. Huang, J.S. Zhou, R. Xu, *JACS* 133 (2011) 20680–20683.
- [126] D.-Y. Wang, M. Gong, H.L. Chou, C.J. Pan, H.A. Chen, Y. Wu, M.C. Lin, M. Guan, J. Yang, C.W. Chen, *JACS* 137 (2015) 1587–1592.
- [127] T. Lazarides, T. McCormick, P. Du, G. Luo, B. Lindley, R. Eisenberg, *JACS* 131 (2009) 9192.
- [128] J. Song, X. Gu, J. Cheng, N. Fan, H. Zhang, H. Su, *Appl. Catal. B: Environ.* 225 (2018) 424–432.
- [129] D. Sun, V. Mazumder, Ö. Metin, S. Sun, *ACS Nano* 5 (2011) 6458–6464.
- [130] L. Guo, X. Gu, K. Kang, Y. Wu, J. Cheng, P. Liu, T. Wang, H. Su, *J. Mater. Chem. A* 3 (2015) 22807–22815.
- [131] S. Akbayrak, M. Kaya, M. Volkan, S. Özkaz, *Appl. Catal. B: Environ.* 147 (2014) 387–393.
- [132] J.C. Védrine, *ChemSusChem* 12 (2019) 577–588.
- [133] S. Dang, Q.-L. Zhu, Q. Xu, *Nat. Rev. Mater.* 3 (2017) 17075.
- [134] D. Huang, Z. Hu, Z. Peng, G. Zeng, G. Chen, C. Zhang, M. Cheng, J. Wan, X. Wang, X. Qin, *J. Environ. Manage.* 210 (2018) 191–200.
- [135] H. Wang, Y. Wu, T. Xiao, X. Yuan, G. Zeng, W. Tu, S. Wu, H.Y. Lee, Y.Z. Tan, J.W. Chew, *Appl. Catal. B: Environ.* 233 (2018) 213–225.
- [136] Z. Liang, C. Qu, W. Guo, R. Zou, Q. Xu, *Adv. Mater.* 30 (2018) 1702891.
- [137] X. Yang, A. Wolcott, G. Wang, A. Sobo, R.C. Fitzmorris, F. Qian, J.Z. Zhang, Y. Li, *Nano Lett.* 9 (2009) 2331–2336.
- [138] T. Xu, L. Zhang, H. Cheng, Y. Zhu, *Appl. Catal. B: Environ.* 101 (2011) 382–387.
- [139] S. Chakrabarti, B.K. Dutta, J. Hazard. Mater. 112 (2004) 269–278.
- [140] R. Georgekutty, M.K. Seery, S.C. Pillai, *J. Phys. Chem. C* 112 (2008) 13563–13570.
- [141] D.-L. Huang, C. Wang, P. Xu, G.-M. Zeng, B.-A. Lu, N.-J. Li, C. Huang, C. Lai, M.-H. Zhao, J.-J. Xu, X.-Y. Luo, *Int. Biodeterior. Biodegrad.* 97 (2015) 115–123.
- [142] H. Wang, X. Yuan, Y. Wu, X. Chen, L. Leng, H. Wang, H. Li, G. Zeng, *Chem. Eng. J.* 262 (2015) 597–606.
- [143] J. Theerthagiri, S. Chandrasekaran, S. Salla, V. Elakkiya, R.A. Senthil, P. Nithyadharseni, T. Maiyalagan, K. Micheal, A. Ayeshamariam, M.V. Arasu, N.A. Al-Dhabi, H.-S. Kim, *J. Solid State Chem.* 267 (2018) 35–52.
- [144] C. Yu, W. Zhou, H. Liu, Y. Liu, D.D. Dionysiou, *Chem. Eng. J.* 287 (2016) 117–129.
- [145] O. Sacco, V. Vaiano, C. Han, D. Sannino, D.D. Dionysiou, *Appl. Catal. B: Environ.* 164 (2015) 462–474.
- [146] Y. Liu, X. He, Y. Fu, D.D. Dionysiou, *Chem. Eng. J.* 284 (2016) 1317–1327.
- [147] M. Cheng, G. Zeng, D. Huang, C. Yang, C. Lai, C. Zhang, Y. Liu, *Crit. Rev. Biotechnol.* 38 (2018) 17–30.
- [148] M. Cheng, G. Zeng, D. Huang, C. Lai, P. Xu, C. Zhang, Y. Liu, *Chem. Eng. J.* 284 (2016) 582–598.
- [149] Z. Liu, B. Shao, G. Zeng, M. Chen, Z. Li, Y. Liu, Y. Jiang, H. Zhong, Y. Liu, M. Yan, *Chemosphere* 210 (2018) 922–930.
- [150] Y. Ma, Z. Li, *Appl. Surf. Sci.* 452 (2018) 279–285.
- [151] M. Wang, D. Wang, Z. Li, *Appl. Catal. B: Environ.* 183 (2016) 47–52.
- [152] R. Chandra, S. Mukhopadhyay, M. Nath, *Mater. Lett.* 164 (2016) 571–574.
- [153] N. Chang, H. Zhang, M.-S. Shi, J. Li, W. Shao, H.-T. Wang, *Mater. Lett.* 200 (2017) 55–58.
- [154] X. Li, Y. Pi, Q. Xia, Z. Li, J. Xiao, *Appl. Catal. B: Environ.* 191 (2016) 192–201.
- [155] X. Li, Y. Pi, Q. Hou, H. Yu, Z. Li, Y. Li, J. Xiao, *Chem. Commun.* 54 (2018) 1917–1920.
- [156] X. Liu, R. Dang, W. Dong, X. Huang, J. Tang, H. Gao, G. Wang, *Appl. Catal. B: Environ.* 209 (2017) 506–513.
- [157] D. Huang, X. Wang, C. Zhang, G. Zeng, Z. Peng, J. Zhou, M. Cheng, R. Wang, Z. Hu, X. Qin, *Chemosphere* 186 (2017) 414–421.
- [158] X. Zeng, L. Huang, C. Wang, J. Wang, J. Li, X. Luo, *ACS Appl. Mater. Interfaces* 8 (2016) 20274.
- [159] U.P.N. Tran, K.K.A. Le, N.T.S. Phan, *ACS Catal.* 1 (2016) 120–127.
- [160] Y. Liu, G. Zeng, H. Zhong, Z. Wang, Z. Liu, M. Cheng, G. Liu, X. Yang, S. Liu, J. Hazard. Mater. 322 (2017) 394–401.
- [161] P. Horcajada, S. Surblé, C. Serre, D.Y. Hong, Y.K. Seo, J.S. Chang, J.M. Grenèche, I. Margiolaki, G. Férey, *Chem. Commun.* 27 (2007) 2820–2822.
- [162] W.-W. Zhan, Q. Kuang, J.-Z. Zhou, X.-J. Kong, Z.-X. Xie, L.-S. Zheng, *JACS* 135 (2013) 1926–1933.
- [163] J. Cravillon, R. Nayuk, S. Springer, A. Feldhoff, K. Huber, M. Wiebcke, *Chem. Mater.* 23 (2011) 2130–2141.
- [164] Y. Pan, D. Heryadi, F. Zhou, L. Zhao, G. Lestari, H. Su, Z. Lai, *CrystEngComm* 13 (2011) 6937–6940.
- [165] Y. Pan, Y. Liu, G. Zeng, L. Zhao, Z. Lai, *Chem. Commun.* 47 (2011) 2071–2073.
- [166] S.R. Venna, J.B. Jasinski, M.A. Carreon, *JACS* 132 (2010) 18030–18033.
- [167] M. Rad, S. Dehghanpour, *RSC Adv.* 6 (2016).
- [168] B. Yu, F. Wang, W. Dong, J. Hou, P. Lu, J. Gong, *Mater. Lett.* 156 (2015) 50–53.
- [169] G. Jia, L. Liu, L. Zhang, D. Zhang, Y. Wang, X. Cui, W. Zheng, *Appl. Surf. Sci.* 448 (2018).
- [170] L. Lin, H. Liu, X. Zhang, *Chem. Eng. J.* 328 (2017) 124–132.
- [171] X.X. Xu, Z.P. Cui, J. Qi, X.X. Liu, *DTr* 42 (2013) 4031–4039.
- [172] X. Wang, J. Liu, S. Leong, X. Lin, J. Wei, B. Kong, Y. Xu, Z.-X. Low, J. Yao, H. Wang, *ACS Appl. Mater. Interfaces* 8 (2016) 9080–9087.
- [173] C. Zhang, C. Lai, G. Zeng, D. Huang, C. Yang, Y. Wang, Y. Zhou, M. Cheng, *Water Res.* 95 (2016) 103–112.
- [174] D. Huang, W. Xue, G. Zeng, J. Wan, G. Chen, C. Huang, C. Zhang, M. Cheng, P. Xu, *Water Res.* 106 (2016) 15–25.
- [175] C. Hu, D. Huang, G. Zeng, M. Cheng, X. Gong, R. Wang, W. Xue, Z. Hu, Y. Liu, *Chem. Eng. J.* 338 (2018) 432–439.
- [176] L. Jiao, Y. Wang, H.L. Jiang, Q. Xu, *Adv. Mater.* (2017) 1703663.
- [177] M.E. Silvestre, M. Franzreb, P.G. Weidler, O. Shekhah, C. Wöll, *Adv. Funct. Mater.* 23 (2013) 1210–1213.
- [178] F. Ke, L.G. Qiu, J. Zhu, *Nanoscale* 6 (2014) 1596–1601.
- [179] Z. Miao, F. Yang, L. Yi, X. Shu, D. Ramella, *J. Solid State Chem.* 256 (2017).
- [180] C.-F. Zhang, L.-G. Qiu, F. Ke, Y.-J. Zhu, Y.-P. Yuan, G.-S. Xu, X. Jiang, *J. Mater. Chem. A* 1 (2013) 14329–14334.
- [181] X. Yue, W. Guo, X. Li, H. Zhou, R. Wang, *Environ. Sci. Pollut. Res.* 23 (2016) 15218–15226.
- [182] L. Zhang, W. Wang, L. Zhou, M. Shang, S. Sun, *Appl. Catal. B: Environ.* 90 (2009) 458–462.
- [183] G. Xi, B. Yue, J. Cao, J. Ye, *Chem. A Eur. J.* 17 (2011) 5145–5154.
- [184] J.-F. Guo, B. Ma, A. Yin, K. Fan, W.-L. Dai, *Appl. Catal. B: Environ.* 101 (2011) 580–586.
- [185] X. Gong, D. Huang, Y. Liu, Z. Peng, G. Zeng, P. Xu, M. Cheng, R. Wang, J. Wan, *Crit. Rev. Biotechnol.* 38 (2018) 455–468.
- [186] H. Zhao, L. Qian, H. Lv, Y. Wang, G. Zhao, *ChemCatChem* 7 (2016) 4148–4155.
- [187] M. Cheng, G. Zeng, D. Huang, C. Lai, Y. Liu, P. Xu, C. Zhang, J. Wan, L. Hu, W. Xiong, *C. Zhou, Chem. Eng. J.* 327 (2017) 686–693.
- [188] M. Cheng, G. Zeng, D. Huang, C. Lai, Y. Liu, C. Zhang, J. Wan, L. Hu, C. Zhou, W. Xiong, *Water Res.* 138 (2018) 7–18.
- [189] M. Cheng, G. Zeng, D. Huang, C. Yang, C. Lai, C. Zhang, Y. Liu, *Chem. Eng. J.* 314 (2017) 98–113.
- [190] X. Zong, H. Yan, G. Wu, G. Ma, F. Wen, L. Wang, C. Li, *JACS* 130 (2008) 7176.
- [191] Q. Li, B. Guo, J. Yu, J. Ran, B. Zhang, H. Yan, J.R. Gong, *JACS* 133 (2011) 10878–10884.
- [192] Y. Su, D. Ao, H. Liu, Y. Wang, *J. Mater. Chem. A* 5 (2017) 8680–8689.
- [193] N. Qin, J. Xiong, R. Liang, Y. Liu, S. Zhang, Y. Li, Z. Li, L. Wu, *Appl. Catal. B: Environ.* 202 (2017) 374–380.
- [194] J. He, Z. Yan, J. Wang, J. Xie, L. Jiang, Y. Shi, F. Yuan, F. Yu, Y. Sun, *Chem. Commun.* 49 (2013) 6761–6763.
- [195] J. He, H. Yang, Y. Chen, Z. Yan, Y. Zeng, Z. Luo, W. Gao, J. Wang, *Water Air Soil Pollut.* 226 (2015) 197.
- [196] F. Ke, L. Wang, J. Zhu, *Nano Res.* 8 (2015) 1834–1846.
- [197] R. Lin, L. Shen, Z. Ren, W. Wu, Y. Tan, H. Fu, J. Zhang, L. Wu, *Chem. Commun.* 50 (2014) 8533–8535.
- [198] J.-J. Zhou, R. Wang, X.-L. Liu, F.-M. Peng, C.-H. Li, F. Teng, Y.-P. Yuan, *Appl. Surf. Sci.* 346 (2015) 278–283.
- [199] L. Shen, M. Luo, Y. Liu, R. Liang, F. Jing, L. Wu, *Appl. Catal. B: Environ.* 166–167 (2015) 445–453.
- [200] M. Zeng, Z. Chai, X. Deng, Q. Li, S. Feng, J. Wang, D. Xu, *Nano Res.* 9 (2016) 1–6.
- [201] A. Rahmani, H.B.M. Emrooz, S. Abedi, A. Morsali, *Mater. Sci. Semicond. Process.* 80 (2018) 44–51.
- [202] Q. Liang, S. Cui, C. Liu, S. Xu, C. Yao, Z. Li, *J. Colloid Interface Sci.* 524 (2018).
- [203] K.M. Cho, K.H. Kim, K. Park, C. Kim, S. Kim, A. Al-Saggaf, I. Gereige, H.-T. Jung, *ACS Catal.* 7 (2017) 7064–7069.
- [204] Z. Liu, Z. Wang, S. Qing, N. Xue, S. Jia, L. Zhang, L. Li, N. Li, L. Shi, J. Chen, *Appl. Catal. B: Environ.* 232 (2018) 86–92.
- [205] M.M. Kandy, V.G. Gaikar, *Mater. Res. Bull.* 102 (2018) 440–449.
- [206] J. Jin, J. Yu, D. Guo, C. Cui, W. Ho, *Small* 11 (2015) 5262–5271.
- [207] S. Wang, X. Wang, *Appl. Catal. B: Environ.* 162 (2015) 494–500.
- [208] Y. Su, Z. Zhang, H. Liu, Y. Wang, *Appl. Catal. B: Environ.* 200 (2017) 448–457.
- [209] H. Zhao, X. Yang, R. Xu, J. Li, S. Gao, R. Cao, *J. Mater. Chem. A* 6 (2018) 20152–20160.
- [210] C. Chen, T. Wu, H. Wu, H. Liu, Q. Qian, Z. Liu, G. Yang, B. Han, *Chem. Sci.* 9 (2018) 8890–8894.
- [211] H. Zhang, J. Wei, J. Dong, G. Liu, L. Shi, P. An, G. Zhao, J. Kong, X. Wang, X. Meng, *Angew. Chem.* 128 (2016) 14522–14526.
- [212] L. Shi, T. Wang, H. Zhang, K. Chang, J. Ye, *Adv. Funct. Mater.* 25 (2015) 5360–5367.
- [213] S. Wang, B.Y. Guan, Y. Lu, X.W.D. Lou, *JACS* 139 (2017) 17305–17308.
- [214] S. Gao, T. Feng, C. Feng, N. Shang, C. Wang, *J. Colloid Interface Sci.* 466 (2016) 284–290.
- [215] J. Liu, R. Li, Y. Hu, T. Li, Z. Jia, Y. Wang, Y. Wang, X. Zhang, C. Fan, *Appl. Catal. B: Environ.* 202 (2017) 64–71.
- [216] J. Liu, R. Li, Y. Wang, Y. Wang, X. Zhang, C. Fan, *J. Alloys Compd.* 693 (2017) 543–549.
- [217] Y. Yang, Z. Zeng, C. Zhang, D. Huang, G. Zeng, R. Xiao, C. Lai, C. Zhou, H. Guo, W. Xue, *Chem. Eng. J.* 349 (2018) 808–821.
- [218] R.M. Abdelhameed, D.M. Tobaaldi, M. Karmaoui, *J. Photochem. Photobiol. A Chem.* 351 (2018) 50–58.
- [219] J. Yu, G. Dai, B. Huang, *J. Phys. Chem. C* 113 (2009) 16394–16401.
- [220] Y. Tang, V.P. Subramaniam, T.H. Lau, Y. Lai, D. Gong, P.D. Kanhere, Y.H. Cheng, Z. Chen, Z. Dong, *Appl. Catal. B: Environ.* 106 (2011) 577–585.
- [221] R. Dong, B. Tian, C. Zeng, T. Li, T. Wang, J. Zhang, *J. Phys. Chem. C* 117 (2013) 213–220.

- [222] Y. Liu, Z. Liu, G. Zeng, M. Chen, Y. Jiang, B. Shao, Z. Li, Y. Liu, *J. Hazard. Mater.* 357 (2018) 10–18.
- [223] J. Yan, W.-Z. Zhou, H. Tan, X.-J. Feng, Y.-H. Wang, Y.-G. Li, *CrystEngComm* 18 (2016) 8762–8768.
- [224] Q. Liu, C. Zeng, L. Ai, Z. Hao, J. Jiang, *Appl. Catal. B: Environ.* 224 (2018) 38–45.
- [225] Y. Wen, J. Zhang, Q. Xu, X.-T. Wu, Q.-L. Zhu, *Coord. Chem. Rev.* 376 (2018) 248–276.
- [226] Y.-J. Tang, Y. Chen, H.-J. Zhu, A.M. Zhang, X.-L. Wang, L.-Z. Dong, S.-L. Li, Q. Xu, Y.-Q. Lan, *J. Mater. Chem. A* 6 (2018) 21969–21977.
- [227] M. Blasco-Ahicart, J. Soriano-Lopez, J.J. Carbo, J.M. Poblet, J.R. Galan-Mascaros, *Nat. Chem.* 10 (2018) 24–30.
- [228] M. Stuckart, K.Y. Monakhov, *J. Mater. Chem. A* 6 (2018) 17849–17853.
- [229] Z.-M. Zhang, T. Zhang, C. Wang, Z. Lin, L.-S. Long, W. Lin, *JACS* 137 (2015) 3197–3200.
- [230] G. Paille, M. Gomez-Mingot, C. Roch-Marchal, B. Lassalle-Kaiser, P. Mialane, M. Fontecave, C. Mellot-Draznieks, A. Dolbecq, *JACS* 140 (2018) 3613–3618.
- [231] J. Tian, B. Lin, Y. Sun, X. Zhang, H. Yang, *Mater. Lett.* 206 (2017) 91–94.
- [232] X.-J. Kong, Z. Lin, Z.-M. Zhang, T. Zhang, W. Lin, *Angew. Chem. Int. Ed.* 55 (2016) 6411–6416.
- [233] J. Han, D. Wang, Y. Du, S. Xi, Z. Chen, S. Yin, T. Zhou, R. Xu, *Appl. Catal. A: Gen.* 521 (2016) 83–89.
- [234] Q. Lan, Z.-M. Zhang, C. Qin, X.-L. Wang, Y.-G. Li, H.-Q. Tan, E.-B. Wang, *Chem. A Eur. J.* 22 (2016) 15513–15520.